Therefore, we performed whole-exome sequencing (WES) combined, when applicable, with autozygome analysis to identify mutations in novel genes that underlie the disease pathology in a cohort of individuals affected with NM with unknown genetic diagnosis. All subjects were enrolled following informed consent and research was conducted according to the protocols approved by the Institutional Review Boards of the respective institutions in which these individuals were recruited. Molecular screening was performed on genomic DNA isolated from blood samples following standard protocols.

We performed whole-exome or whole-genome sequencing on a cohort of 60 unrelated NM probands through Boston Children's Hospital Gene Partnership facility. Molecular screening was performed on genomic DNA isolated from blood samples with standard protocols. Whole-blood DNA was subjected to solution capture (SureSelect Human All Exon V4, Agilent Technologies) to generate barcoded whole-exome sequencing libraries. Libraries were sequenced on an Illumina HiSeq 2000, employing paired end reads (100 bp × 2) to a mean target coverage of 96.5% and a mean read depth of 71.6. Alignment, variant calling, and annotation were performed with a custom informatics pipeline employing BWA,[14] Picard, and ANNOVAR[15] focusing on rare (<3% in db SNP135, 1000 Genomes Project Database, and the [EVS] National Heart, Lung, and Blood Institute Exome Sequencing Project Exome Variant Server) protein affecting changes in known and novel human disease genes. Alternatively, probands for families 203 and 832 were sequenced to greater than 50× depth by Axeq Technologies on an Illumina HiSeq 2000 following Agilent SureSelect Exome enrichment with their standard Exome Sequencing service. Whole-exome sequencing identified homozygous mutations of *KLHL41* in two unrelated families, suggesting this gene to be a candidate for NM. All *KLHL41* mutations are numbered relative to the mRNA sequence NM_006063.2 (where position 1 is the first base of the initiating MET codon) and protein NP_006054.2. Family 1 is a nonconsanguineous family of Vietnamese origin. Proband 203-1 is a 16-year-old female with an intermediate form of NM with a high-arched palate, dysarthria, and scoliosis who has required ventilatory support since childhood. WES identified an apparently homozygous c.103T>C transition in exon 1 resulting in a p.Cys35Arg substitution in this individual (Figure 1A). This variant was present as heterozygous in the father and absent in the mother. Copy number analysis in the affected region showed a heterozygous deletion in the mother and the proband, c.(?_-77)_(*602_?)del. Therefore, individual 203-1 is compound heterozygous for a deletion involving a portion of *KLHL41* and a KLHL41 p.Cys35Arg missense change. The second proband (832-1), who is adopted of Russian origin, is ambulant at age 12 and exhibits the typical congenital form of NM. WES identified a homozygous deletion of one base and an insertion of four bases c.459delinsACTC in the proband resulting in a single amino acid insertion, p.Ser153_Ala154insLeu in the protein (Figure 1A).

Whole-exome sequencing in probands with severe NM in Australian and Saudi Arabian cohorts resulted in identification of *KLHL41* mutations in two further families. The first (6462) is a consanguineous family of Persian origin from Afghanistan with one child (D12-203) affected with severe NM and four unaffected children (see Figure S1 available online). Homozygosity mapping was performed on the proband with the Illumina HumanCytoSNP-12 array, and the only known NM loci found within homozygous regions were *CFL2* (MIM 601443) and *NEB* (MIM 161650); however, both were excluded following Sanger sequencing, as was *ACTA1* (MIM 102610), which is the most common cause of simplex NM cases. WES of DNA from proband D12-203 was performed at the Lotterywest Sate Biomedical Facility Genomics Node, Royal Perth Hospital, Western Australia.[13] WES identified 453 heterozygous or homozygous variants. Application of the homozygosity data to the list of candidates reduced this to seven candidate variants. Two of these seven candidate variants were in skeletal-muscle-specific genes and of these the most likely candidate was a homozygous deletion within *KLHL41* (chr2: 170382132–170382139; c.1748_1755delAAGGAAAT, p.Lys583Thrfs*7) (Figure 1A). The deletion was confirmed by Sanger sequencing. Both parents and two unaffected siblings were heterozygous for the deletion, and two further unaffected siblings were homozygous for the normal allele.

Family 12DG1177, from a Saudi Arabian cohort is consanguineous (Figure S1). The male proband (12DG1177-1) was a newborn with severe hypotonia, dislocation of hips and knees, and facial dysmorphism in the form of micrognathia and cleft palate. There was a positive family history of two previous sibs who died of unknown causes soon after birth, as well as three healthy living sibs. The proband died of cardiorespiratory arrest shortly after intubation at less than 24 hr of age. Exome capture was performed with TruSeq Exome Enrichment kit (Illumina) as described earlier.[16] Only novel coding and splicing homozygous variants within the autozygome of the affected individual were considered. After filtering, 8,653 homozygous, coding, or splice variants were present, and autozygosity mapping, dbSNP, and analysis of 240 control Saudi exomes finally led to the identification of 18 candidate variants. The only truncating change was a single base deletion in *KLHL41* (c.641delA). This deletion was present in the coding region of exon 1 of *KLHL41* resulting in the frameshift change p.Asn214Thrfs*14 (Figure 1A).

Subsequent screening for *KLHL41* mutations in 116 individuals affected with severe, intermediate, or typical congenital forms of NM in the Boston and Australian NM Cohorts by Sanger sequencing identified a further family (D10-236) with compound heterozygous mutation (c.581_583delAAG, p.Glu194del and c.1238C>T, p.Ser413Leu) in proband. This individual is of Chinese

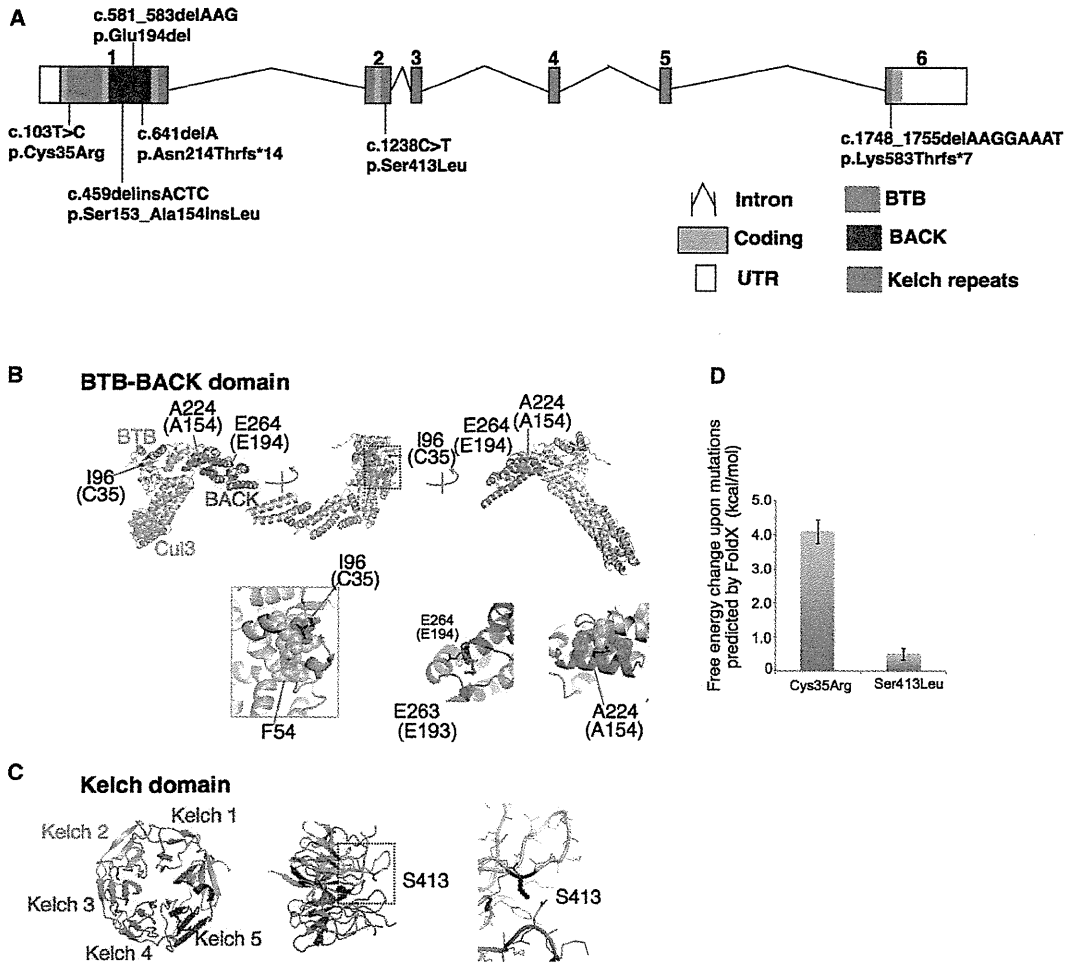

Figure 1. Overview of Mutations in *KLHL41* and Their Effect on Protein Structure

(A) Schematic representation of mutations in *KLHL41*. Boxes represent exons 1–6. Conserved domains of KLHL41 are indicated as follows: BTB (blue), BACK (red), and Kelch repeats (green). The BTB and BACK domains are encoded by exon 1 and the five Kelch repeats are encoded by exons 1–6.

(B and C) Crystal structures of the BTB-BACK domain of human Kelch-like protein (KLHL11) in complex with CUL3 (Protein Data Bank code 4AP2) (B) and the Kelch domain of rat KLHL41 (PDB code 2WOZ) (C). α helices, β strands, and loops are drawn as ribbons, arrows, and threads, respectively. The squared areas correspond to the close-up views in the insets. In (B), the BTB and BACK domains are colored pink and green, respectively, whereas CUL3 is colored yellow, except that Ile96, Ala224, and Glu264 (Cys35, Ala154, and Glu194 in human KLHL41, respectively) are colored red. The side chains of these residues and Glu263 (Glu193 in human KLHL41) are shown as sticks with the indications of amino acid numbers for human KLHL11 and those for human KLHL41 in parentheses. Side chains involved in hydrophobic cores around Ile96 and Ala224 are drawn in van der Waal's representation. In (C), the Kelch domain is color-coded to indicate each Kelch repeat, except that Ser413 is colored red. The side chain of Ser413 is shown as sticks. Molecular structures are drawn with PyMOL.

(D) Predicted free energy changes upon the substitutions of KLHL41 with FoldX software.

origin and exhibited the typical congenital form of NM. The detailed clinical features of affected individuals with mutations identified in *KLHL41* are presented in Table 1.

Overall, WES and Sanger sequencing resulted in identification of seven different mutations in Kelch-like family member 41 (*KLHL41*), previously known as *KBTBD10*, sarcosin, or *KRP1*, in affected NM individuals from five unrelated families (Figure 1A). Muscle histology was typical for NM: biopsies from probands of three different families (D12-203, 832-1, and 10-236) exhibited abnormal Gomori trichrome staining with presence of sarcoplasmic rods that varied from numerous small rods to fewer large rods in multiple myofibers (Figure 2A). No intranuclear rods or cores were seen. The missense changes identified in *KLHL41* are predicted to be pathogenic by polyphen, SIFT and pMUT and the mutated amino-acid residues are conserved in all representative species during evolution (Figure S2). The neighboring areas surrounding the sites of insertion or deletion are also relatively conserved, suggesting a structural or functional requirement for the altered amino acid residues (Figure S2). Sequencing of family members revealed that *KLHL41*

Table1. Clinical Manifestations in Affected Individuals Harboring *KLHL41* Mutations

Proband ID	cDNA Change	Amino Acid Change	Clinical Category	Sex	Nationality	Pregnancy and Delivery	Alive at Age/Mobility/ Age at Death	Associated Features
203-1	c.103T>C c.(?_-77)_(*602_?)del	p.Cys35Arg Heterozygous p.0? Heterozygous	Intermediate	F	Vietnamese	Normal	16 yrs, uses wheelchair (ambulant 24–36 mo)	Ventilated 24 hr from 5 yrs. High-arched palate, dysarthria Scoliosis
832-1	c.459delinsACTC	p.Ser153_Ala154insLeu Homozygous	Other forms (grade of severity: mild)	M	Russian	No data	12 yrs, ambulant	Distal weakness > proximal distal contractures
D10-236	c.581_583delAAG c.1238C>T	p.Glu194del Heterozygous p.Ser413Leu Heterozygous	Typical form	M	Chinese	Normal - h 40	5 yrs, ambulant	VSD, finger contractures, focal renal echogenicity
D12-203	c.1748_1755del AAGGAAAT,	p.Lys583Thrfs*7 Homozygous	Fetal akinesia sequence	M	Persian	Polyhydramnios, breech presentation, emergency Cesarean section - h 31+2	Died at 3 mo (active support discontinued)	Arthrogryposis, macrocephaly, hypospadias No antigravity movements at birth
12DG1177	c.641delA	p.Asn214Thrfs*14 Homozygous	Severe form Fetal akinesia sequence	M	Saudi Arabian	Fetal movements weak, breech presentation	Died during 1st day of life	Dislocation of hips and knees, cleft palate, micrognathia, narrow chest

mutations showed a segregation pattern compatible with a recessive mode of inheritance in all families (Figure S1). Severe phenotypes associated with genetic null mutations and intermediate or typical congenital forms with mutations that should results in presence of residual protein, suggests a phenotype-genotype correlation in individuals affected with *KLHL41* mutations.

KLHL41 belongs to the family of BTB-Kelch domain-containing proteins.[17–20] Mutations in two other members of this family, *KBTBD13* (MIM 613727), and most recently *KLHL40* (MIM 615430), have been associated with a clinically distinct form of congenital myopathy exhibiting nemaline bodies, as well as multiminicores and severe NM, respectively.[12,13] To evaluate the impacts of the *KLHL41* mutations on the protein structure, we mapped them onto the crystal structures of the BTB-BACK domain of human KLHL11 in complex with human CUL3, a subunit of E3 ubiquitin ligases, (PDB code 4AP2)[21] and the Kelch domain of rat KLHL41 (PDB code 2WOZ),[22] analogous to those domains of human KLHL41. The Cys35 side chain is involved in a hydrophobic core of the BTB domain, which makes van der Waals contacts with Phe54 of Cul3 (Figure 1B). The p.Cys35Arg substitution present in affected individual 203-1 would likely destabilize the hydrophobic core and thereby impair the interaction with Cul3. This was supported by the FoldX result, in which free energy change upon the p.Cys35Arg substitution was predicted to be over 4 kcal/mol, which can be interpreted as considerable destabilization of a protein structure (Figure 1D; Figure S3).[23] In proband 832-1, a Leu residue is inserted between the amino acid positions 153 and 154 in the center of a helix, in which several residues are involved in a hydrophobic core of the BACK domain (Figure 1B). This amino acid insertion is likely to destabilize the BACK domain fold. In proband D10-236, the p.Ser413Leu substitution was mapped to a loop region, which is located near the substrate-binding region of the Kelch repeat 2 (Figure 1C; Figure S1B). A FoldX calculation predicted that the p.Ser413Leu substitution would have minimal effect on stability of the Kelch domain (Figure 1D). The effect of Glu194 deletion at the N-terminal end of an α helix can be compensated by the presence of Glu193 located in the loop (Figure 1B). Nonetheless, it cannot be excluded that the p.Ser413Leu and p.Glu194del changes alter the protein solubility or aggregate tendency and/or impair substrate binding. The conserved nature of the mutated KLHL41 domains, as well as the potential role of the mutations in disrupting those structural domains, supports the likely pathogenicity of these mutations.

The localization of KLHL41 in skeletal muscles was investigated by immunofluorescence of mouse FDB cultured myofibers and human skeletal muscle cryosections. Immunofluorescence with two different antibodies against N-terminal (Sigma, AV38732) and C-terminal parts of human KLHL41 (Abcam, ab66605) was performed, and z stacks were acquired by confocal microscopy as described

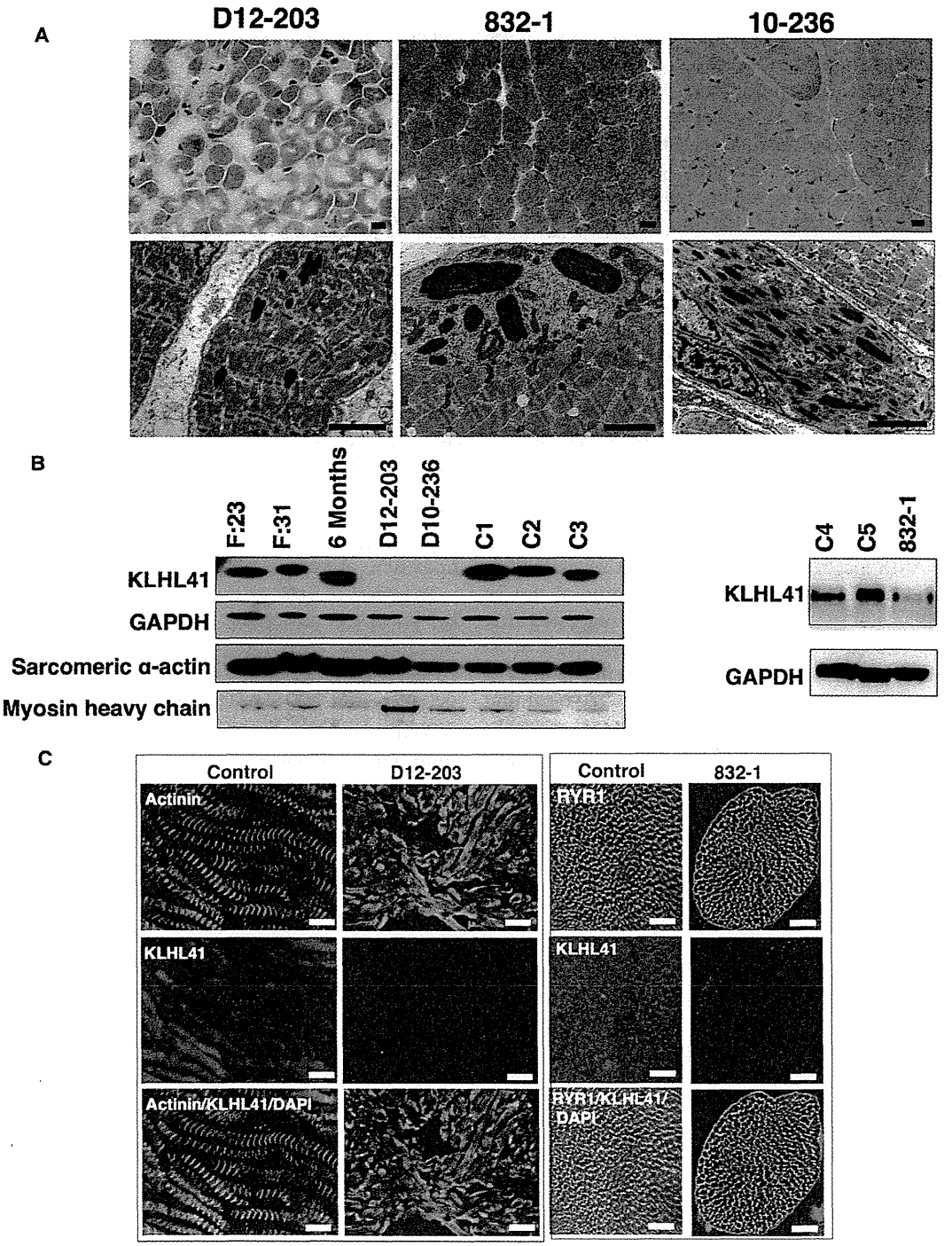

Figure 2. Muscle Pathology and Expression of KLHL41 Levels and Localization in Muscle of Affected Individuals
(A) Light microscopy of Gomori trichrome stained skeletal muscle from affected individuals with *KLHL41* mutations show cytoplasmic nemaline bodies (top panel). Electron microscopy of affected muscles reveals rods of variable frequency and size and severe myofibrillar disarray (bottom panels). (Scale bars represent 2 μm). Affected individuals' IDs are indicated at top.
(B) Immunoblotting analysis of KLHL41 levels in affected and unaffected muscles. A decrease in protein levels was observed in individuals with *KLHL41* mutations in comparison to normal control muscles. Immunoblotting with sarcomeric actin or Coomassie staining of myosin heavy chain showed no abnormal accumulation of sarcomeric proteins in affected muscles. Immunostaining for GAPDH was used for loading controls. Lanes: F:23, 23 week control fetus; F:30, 31 week control fetus; 6-month-old control baby, C1–C5 are normal age-matched control muscles.
(C) Immunofluorescence for KLHL41 in control and affected individual muscle biopsies showed highly reduced levels of KLHL41 in longitudinally oriented (left) or transverse sections (right) of skeletal muscles from affected individuals. Scale bars represent 50 μm.

previously.[24] Immunofluorescence with both antibodies resulted in similar staining patterns; however, due to lower background staining, the C-terminal antibody was used for further studies. Costaining with sarcomeric markers in longitudinal planes showed that KLHL41 staining predominated over the I-bands of the sarcomere and at perinuclear regions in human biopsies (Figure 2C) and murine cultured myofibers (Figure S4). Analysis of transverse sections of myofibers from control human biopsies revealed KLHL41 staining in a ring pattern around the myofibrils, generally colocalizing with ryanodine receptors (RYR1), which are a marker of the sarcoplasmic reticulum (Figure S5). Together, these observations suggest that KLHL41 localizes over (but not within) I bands, likely in association with the terminal cisternae of the sarcomplasmic reticulum (SR) and longitudinal vesicles of the SR present in the I-band area at the triadic regions (Figure S4). Colocalization studies with the ER marker protein disulfide isomerase (PDI) in myofibers and skeletal muscles further confirmed the localization of KLHL41 in SR-ER membranes (Figures S4). This overall localization pattern is most consistent with localization to the endoplasmic reticulum (ER) around myonuclei and to microdomains of the SR with ER characteristics.[25] Previous studies suggested that the closely related NM protein, KLHL40, localized at A-bands,[13] but double label immunofluorescence studies of both longitudinal and transverse sections here reveal that it appears colocalized with RYR1, around but not within the myofibrils in cultured myofibers and human skeletal muscles in a pattern overlapping, but not identical to, that of KLHL41 (Figures S4 and S5). These associations of proteins whose defects cause NM with the ER/SR contrasts with previously known NM proteins, all of which are sarcomeric thin filament components, with the exception of KBTBD13 whose localization is not well known.

In mouse tissues, immunoblotting detected KLHL41 in skeletal muscle and diaphragm (Figure S6). In cultured murine C2C12 cells, KLHL41 levels increased during differentiation to myotubes (Figure S6). Immunoblotting of affected skeletal muscle extracts revealed greatly reduced levels of KLHL41 in individuals with *KLHL41* mutations (Figure 2B) and immunofluorescence microscopy of affected individuals' skeletal muscles also showed that KLHL41 levels were greatly reduced in their myofibers (Figure 2C).

Cell culture studies have shown that KLHL41 interacts with nebulin, N-RAP (Nebulin-related anchoring protein), and actin in skeletal muscle and promotes the assembly of myofibrils.[26] KLHL41 regulates skeletal muscle differentiation as overexpression or knockdown inhibited C2C12 myoblast differentiation.[27] Knockdown of *Klhl41* in cultured cardiomyocytes resulted in sarcomeric disorganization with thickening of Z-lines as seen in NM.[28] However, the exact functions of KLHL41 in disease pathology are unknown. Recent studies have identified mutations in two other closely related family members *KBTBD13* and *KLHL40* as causes of NM suggesting the crucial requirement for several Kelch family proteins in skeletal muscle function.[12,13] To investigate the functional role of KLHL41 in vertebrate skeletal muscle development, we employed zebrafish as a model system. Zebrafish have two duplicated orthologs (*klhl41a* and *klhl41b*) that share ~80% similarity with *KLHL41*. Zebrafish whole-mount in situ hybridization was performed to study the spatio-temporal expression of these genes during zebrafish development as described previously.[29] Specifically, RNA probes specific for each Klhl41 gene were generated by amplification of the 3′ UTRs from a cDNA library of 2 day postfertilization (dpf) zebrafish embryos, followed by in vitro transcription to generate digoxigenin-labeled antisense transcripts (primer sequences are provided in Table S1). Whole-mount in situ hybridization showed ubiquitous expression of *klhl41a* during early development at 1 dpf, but by 2 dpf, *klhl41a* transcripts were virtually undetectable in the major axial skeletal muscles. In contract, *klhl41b* expression was predominantly seen in striated muscles, and strong expression in heart and skeletal muscles was observed throughout zebrafish development to at least 5 dpf (Figure 3A).

The effect of KLHL41 deficiency in zebrafish was studied by knocking down the Klhl41 genes with antisense morpholinos. Two independent morpholinos targeting an exon-intron spice site and translational start site were designed for both genes (morpholino sequences are provided in Table S2). As initial experiments with both morpholinos for each transcript resulted in similar phenotypes, we performed the remainder of our studies with the splice-site morpholinos (7 ng). *klhl41a* morphants exhibited leaner bodies, smaller eyes, and pericardial edema as seen in other myopathy models (n = 65–110) (Figure 3B).[30,31] Examination of 3 dpf morphants with polarized light showed reduced birefringence in axial skeletal muscles suggesting disorganized skeletal muscle structure (Figure 3B; Figure S7). Knockdown of *klhl41b* resulted in reduced birefringence without any other significant abnormalities (n = 82–132). Targeting both *klhl41a* and *klhl41b* (7 ng each) resulted in curved bodies with a 30% reduction in size along with small eyes and pericardial edema (n = 89–103), compared to fish injected with control morpholino (14ng). *klhl41a* morphant fish die by 3 dpf while *klhl41b* morphants typically did not survive past 5 dpf. Knockdown of both genes was lethal by 3 dpf. Double knockdown fish exhibited severely disorganized muscle (measured by reduced birefringence) compared to controls and either of the single knockdowns. RT-PCR and immunoblotting confirmed the knockdown of *klhl41a* and *klhl41b* transcripts and a reduction in protein levels (Figures 3C and 3D). Overexpression of human *KLHL41* mRNA in the double morphants resulted in a significant increase in the number of surviving fish with normal birefringence suggesting the specificity of morpholino injections and demonstrating the ability of this single evolutionary ortholog to complement both zebrafish genes (Figure 3E). Behavioral characterization of 3

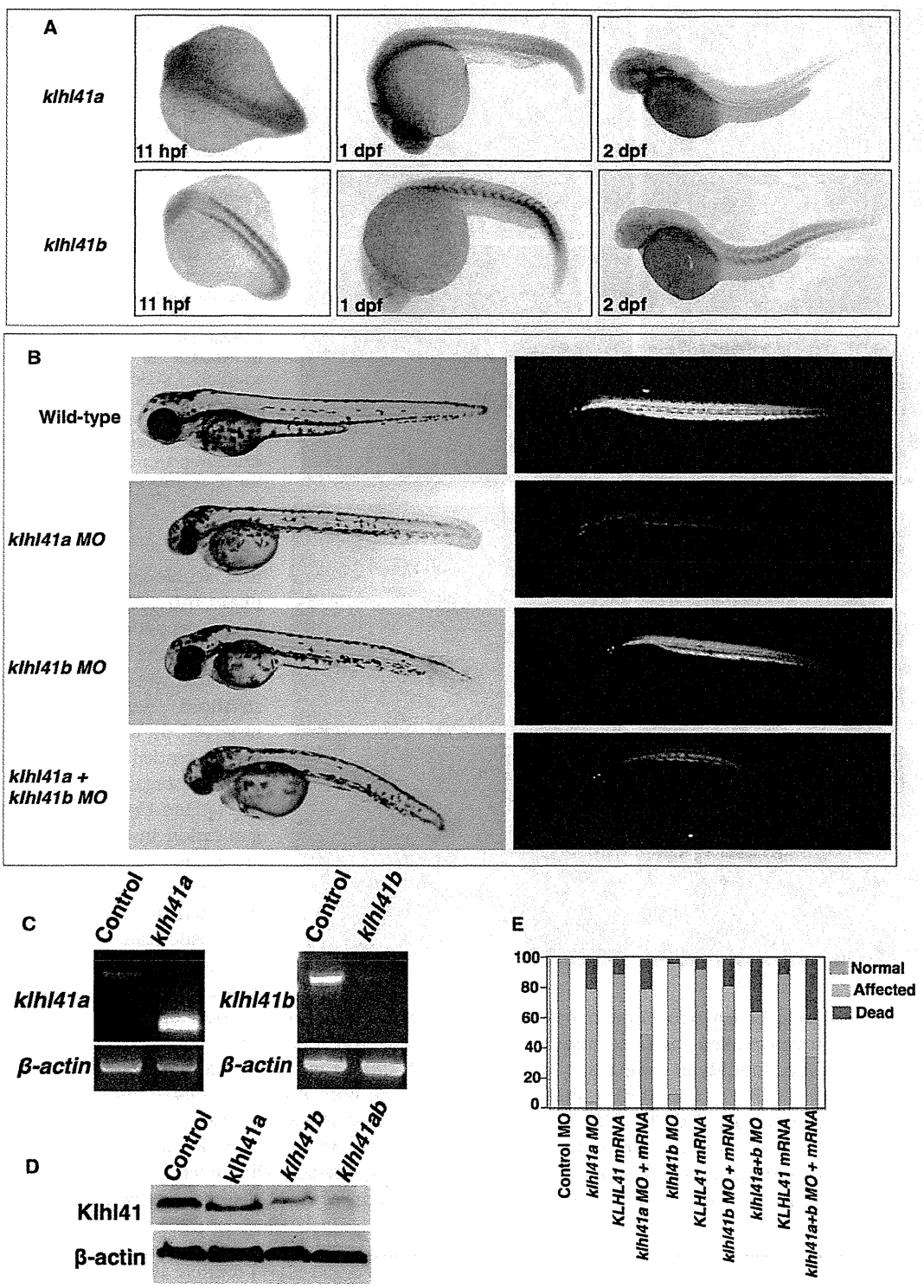

Figure 3. Characterization and Knockdown of Zebrafish Orthologs of *KLHL41*

(A) In situ hybridization of the zebrafish Klhl41 genes shows early expression during myogenesis in developing somites (11 hr after fertilization). *Klhl41a* is expressed in brain, eyes, and muscle at 1 dpf. Later in development expression is largely restricted to brain and heart (2 dpf), although low levels of expression in axial slow skeletal myofibers cannot be excluded due to limited sensitivity of the assay. *Klhl41b* expression is localized to skeletal muscle and heart at all developmental stages (1–2 dpf).

(B) Knockdown of Klhl41 genes in zebrafish using antisense morpholinos results in myopathic changes. Live microscopy of zebrafish embryos at 3 dpf reveals leaner and smaller bodies in comparison to wild-type (WT) fish. Under polarized microscopy, zebrafish embryos

(legend continued on next page)

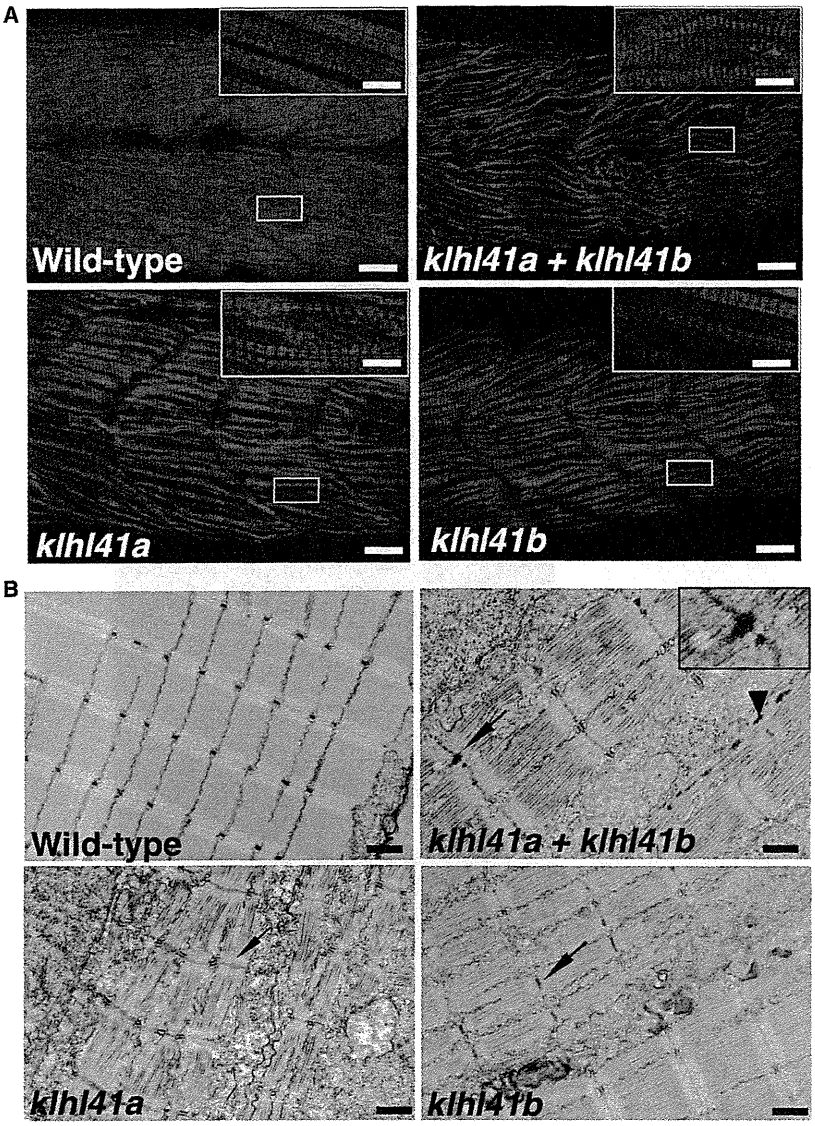

Figure 4. Loss of *klhl41* Function in Zebrafish Recapitulates the Disease Pathology of Human Nemaline Myopathies
(A) Whole-mount staining of 3 dpf zebrafish embryos with phalloidin showed extensive myofibrillar disarray of myofibers in *klhl41* morphant fish (scale bar represents 2 μm). Three dpf embryos fixed in 4% paraformaldehyde were incubated with phalloidin (Invitrogen, A12380, 1:40) overnight at 4°C. Skeletal muscles of klhl41-deficient embryos were smaller and exhibited an overall reduction of myofibrillar organization (inset, high magnification).
(B) Electron microscopy of klhl41-deficient skeletal muscle revealed thickened Z-lines in *klhl41a* or *klhl41b* morphants. In addition, skeletal muscle of double knockdown fish contained electron dense bodies, reminiscent of nascent nemaline rods (arrowhead, nemaline bodies like structures; arrow, thickened Z-lines) (scale bar represents 1 μm).

dpf morphant fish, knocked down for either or both Klhl41 genes, using the touch-evoked response assay showed significantly diminished motility in comparison to control fish (WT fish: 5.74 ± 0.98 cm/0.1 s; *klhl41a*: 1.32 ± 0.61 cm/0.1 s; *klhl41b*: 2.00 ± 0.49 cm/0.1 s; *klhl41ab*: 0.73 ± 0.39 cm/0.1 s), suggesting a significant degree of overall muscle weakness (Movies S1, S2, S3, and S4).[32] To visualize abnormalities in sarcomeric architecture, whole-mount staining of morphant fish and control zebrafish embryos was performed with phalloidin to stain the actin-thin filaments. Although well-organized myofibrillar striations (i.e., sarcomeres) were observed, the myofibrils in *klhl41* morphants tended to be thinner and were highly disorganized relative to control fish (Figure 4A). The myofibrilar disorganization in *klhl41* morphants was also evident by evaluation of ultrathin toluidine blue sections of control and morphant fish (Figure S7). The main diagnostic feature of NM is the presence of nemaline rods with or without Z-line streaming in skeletal muscle. Ultrastructural examination of zebrafish skeletal muscle by electron microscopy showed Z-line thickening in both *klhl41a* and *klhl41b* morphant fish (Figure 4B). Knockdown of both *klhla* and *klhl41b* resulted in the presence of numerous electron-dense structures, reminiscent of small or nascent nemaline bodies, in addition to Z-line thickening (Figure 4B). Given the differences in temporal expression of *klhl41a* (early embryogenesis) and *klhl41b*

exhibit a reduction in birefringence in morphant fish, quantified in ImageJ as described (WT controls: 100% ± 5.9% *klhl41a*: 23% ± 3.0%; *klhl41b*: 31% ± 8.2%; *klhl41ab*: 16% ± 4.2%). Double knockdown fish show a more severe skeletal muscle phenotype than single morphants.
(C) RT-PCR analysis showed knockdown of normal transcripts in the morphant fish.
(D) Immunoblot analysis showed reduction in Klhl41 levels in *klhl41a*, *klhl41b*, and *klhl41ab* fish. Klhl41 antibody recognizes both klhl41a and klhl41b and therefore show immunoreactibility to the other gene in the single morphants that is highly reduced in double morphants.
(E) Overexpression of human *KLHL41* mRNA restores the skeletal muscle phenotypes of *klhl41a/b* single and double morphants suggesting morpholino specificity. The mRNA concentration used to rescue were as follows: *klhl41a* (50 pg), *klhl41b* (75 pg), *klhl41a+b* (60 pg of each).

(maintained later in development), and the high degree of structural and functional conservation (both are rescued by the single human transcript), it is likely that increased severity of *klhl41a* morphants is due to this being the predominant embryonic isoform at the early stages targeted by morpholino injections.

Extensive skeletal muscle disorganization associated with sarcomeric abnormalities in morphant fish points toward a function of KLHL41 in skeletal muscle development and maintenance. Mutations affecting the closely related BTB-Kelch family member KLHL40 have recently also been reported to cause nemaline myopathy.[13] While *KLHL40* mutations resulted in a severe clinical presentation in most of the affected individuals, KLHL41 abnormalities are associated with a spectrum of phenotypes from severe with neonatal death, to survival into late childhood. However, no significant differences were seen in skeletal muscle pathology. KLHL40 contains a putative nuclear localization sequence (NLS) and is expressed throughout muscle differentiation, whereas KLHL41 lacks NLS and is expressed in late differentiation (Figure S8).[13] KLHL41 and many other BTB domain-containing Kelch family members are known to interact with Cul3 ubiquitin ligase to form functional ubiquitination complexes with proteins targeted for degradation.[21,33] KLHL41, which has been shown to interact with nebulin,[34] is now the third BTB-Kelch family member to be identified as a cause of NM when mutated. We hypothesize that improper surveillance and degradation of aberrant thin-filament proteins might explain the convergent pathological and clinical phenotypes associated with mutations of thin filament and BTB-Kelch family member genes in NM.

Supplemental Data

Supplemental Data include eight figures, two tables, and four movies and can be found with this article online at http://www.cell.com/AJHG/home.

Acknowledgments

We are grateful to the many NM affected individuals and their families, and to their treating physicians, for their participation in this research. Whole-exome sequencing was made possible through the generous support and assistance of David Margulies and the entire staff of The Gene Partnership Project at Boston Children's Hospital. We would like to thank Pankaj Agrawal and Wen-Hann Tan for many helpful discussions during the course of this work. We are thankful to Louise Trakimas of the electron microscope facility at Harvard Medical School for excellent help with zebrafish histology, and the Genotyping and Sequencing Core Facilities at KFSHRC for their technical help. V.A.G. is supported by K01 AR062601 from the National Institute of Arthritis and Musculoskeletal and Skin Diseases of National Institute of Health. This work was also supported by the Muscular Dystrophy Association of USA (MDA201302), National Institutes of Health grant from the National Institute of Arthritis and Musculoskeletal and Skin Diseases R01 AR044345, the AUism Charitable Foundation, and A Foundation Building Strength (to A.H.B.); National Health and Medical Research Council of Australia Early Career Researcher Fellowship #1035955 (to G.R.); Research Fellowship APP1002147 and Project Grant APP1022707(to N.G.L.); the Association Française contre les Myopathies (#15734), Dubai-Harvard Foundation for Medical Research Collaborative Research Grant (to F.S.A.); a UWA Collaborative Research Award (G.R.); and the Great Ormond Street Hospital Children's Charity (to F.M.). E.J.T. and K.S.Y. are supported by University of Western Australia Postgraduate Awards. DNA sequencing was performed by the Boston Children's Hospital Genomics Program Molecular Genetics Core, and confocal microscopy was performed at Boston Children's Hospital Intellectual and Developmental Disability Research Center Imaging Core, both supported by National Institutes of Health grant P30 HD18655. The funders had no role in study design, data collection and analysis, decision to publish, or preparation of the manuscript.

Received: August 9, 2013
Revised: October 15, 2013
Accepted: October 22, 2013
Published: November 21, 2013

Web Resources

The URLs for data presented herein are as follows:

1000 Genomes, http://browser.1000genomes.org
dbSNP, http://www.ncbi.nlm.nih.gov/projects/SNP/
NHLBI Exome Sequencing Project (ESP) Exome Variant Server, http://evs.gs.washington.edu/EVS/
Online Mendelian Inheritance in Man (OMIM), http://www.omim.org/
Picard, http://picard.sourceforge.net/
Pymol, http://www.pymol.org

References

1. Wallgren-Pettersson, C., Sewry, C.A., Nowak, K.J., and Laing, N.G. (2011). Nemaline myopathies. Semin. Pediatr. Neurol. *18*, 230–238.
2. Ryan, M.M., Schnell, C., Strickland, C.D., Shield, L.K., Morgan, G., Iannaccone, S.T., Laing, N.G., Beggs, A.H., and North, K.N. (2001). Nemaline myopathy: a clinical study of 143 cases. Ann. Neurol. *50*, 312–320.
3. Wallgren-Pettersson, C. (2002). Nemaline and myotubular myopathies. Semin. Pediatr. Neurol. *9*, 132–144.
4. Sewry, C.A. (2008). Pathological defects in congenital myopathies. J. Muscle Res. Cell Motil. *29*, 231–238.
5. Hutchinson, D.O., Charlton, A., Laing, N.G., Ilkovski, B., and North, K.N. (2006). Autosomal dominant nemaline myopathy with intranuclear rods due to mutation of the skeletal muscle ACTA1 gene: clinical and pathological variability within a kindred. Neuromuscul. Disord. *16*, 113–121.
6. Pelin, K., Hilpelä, P., Donner, K., Sewry, C., Akkari, P.A., Wilton, S.D., Wattanasirichaigoon, D., Bang, M.L., Centner, T., Hanefeld, F., et al. (1999). Mutations in the nebulin gene associated with autosomal recessive nemaline myopathy. Proc. Natl. Acad. Sci. USA *96*, 2305–2310.
7. Nowak, K.J., Wattanasirichaigoon, D., Goebel, H.H., Wilce, M., Pelin, K., Donner, K., Jacob, R.L., Hübner, C., Oexle, K., Anderson, J.R., et al. (1999). Mutations in the skeletal muscle

alpha-actin gene in patients with actin myopathy and nemaline myopathy. Nat. Genet. *23*, 208–212.

8. Laing, N.G., Wilton, S.D., Akkari, P.A., Dorosz, S., Boundy, K., Kneebone, C., Blumbergs, P., White, S., Watkins, H., Love, D.R., et al. (1995). A mutation in the alpha tropomyosin gene TPM3 associated with autosomal dominant nemaline myopathy. Nat. Genet. *9*, 75–79.
9. Tajsharghi, H., Ohlsson, M., Lindberg, C., and Oldfors, A. (2007). Congenital myopathy with nemaline rods and cap structures caused by a mutation in the beta-tropomyosin gene (TPM2). Arch. Neurol. *64*, 1334–1338.
10. Agrawal, P.B., Greenleaf, R.S., Tomczak, K.K., Lehtokari, V.L., Wallgren-Pettersson, C., Wallefeld, W., Laing, N.G., Darras, B.T., Maciver, S.K., Dormitzer, P.R., and Beggs, A.H. (2007). Nemaline myopathy with minicores caused by mutation of the CFL2 gene encoding the skeletal muscle actin-binding protein, cofilin-2. Am. J. Hum. Genet. *80*, 162–167.
11. Johnston, J.J., Kelley, R.I., Crawford, T.O., Morton, D.H., Agarwala, R., Koch, T., Schäffer, A.A., Francomano, C.A., and Biesecker, L.G. (2000). A novel nemaline myopathy in the Amish caused by a mutation in troponin T1. Am. J. Hum. Genet. *67*, 814–821.
12. Sambuughin, N., Yau, K.S., Olivé, M., Duff, R.M., Bayarsaikhan, M., Lu, S., Gonzalez-Mera, L., Sivadorai, P., Nowak, K.J., Ravenscroft, G., et al. (2010). Dominant mutations in KBTBD13, a member of the BTB/Kelch family, cause nemaline myopathy with cores. Am. J. Hum. Genet. *87*, 842–847.
13. Ravenscroft, G., Miyatake, S., Lehtokari, V.L., Todd, E.J., Vornanen, P., Yau, K.S., Hayashi, Y.K., Miyake, N., Tsurusaki, Y., Doi, H., et al. (2013). Mutations in KLHL40 are a frequent cause of severe autosomal-recessive nemaline myopathy. Am. J. Hum. Genet. *93*, 6–18.
14. Li, H., and Durbin, R. (2009). Fast and accurate short read alignment with Burrows-Wheeler transform. Bioinformatics *25*, 1754–1760.
15. Wang, K., Li, M., and Hakonarson, H. (2010). ANNOVAR: functional annotation of genetic variants from high-throughput sequencing data. Nucleic Acids Res. *38*, e164.
16. Alkuraya, F.S. (2012). Discovery of rare homozygous mutations from studies of consanguineous pedigrees. Curr Protoc Hum Genet. *Chapter 6*, Unit 6, 12.
17. Adams, J., Kelso, R., and Cooley, L. (2000). The kelch repeat superfamily of proteins: propellers of cell function. Trends Cell Biol. *10*, 17–24.
18. Dhanoa, B.S., Cogliati, T., Satish, A.G., Bruford, E.A., and Friedman, J.S. (2013). Update on the Kelch-like (KLHL) gene family. Hum. Genomics *7*, 13.
19. du Puy, L., Beqqali, A., van Tol, H.T., Monshouwer-Kloots, J., Passier, R., Haagsman, H.P., and Roelen, B.A. (2012). Sarcosin (Krp1) in skeletal muscle differentiation: gene expression profiling and knockdown experiments. Int. J. Dev. Biol. *56*, 301–309.
20. Gray, C.H., McGarry, L.C., Spence, H.J., Riboldi-Tunnicliffe, A., and Ozanne, B.W. (2009). Novel beta-propeller of the BTB-Kelch protein Krp1 provides a binding site for Lasp-1 that is necessary for pseudopodial extension. J. Biol. Chem. *284*, 30498–30507.
21. Canning, P., Cooper, C.D., Krojer, T., Murray, J.W., Pike, A.C., Chaikuad, A., Keates, T., Thangaratnarajah, C., Hojzan, V., Marsden, B.D., et al. (2013). Structural basis for Cul3 protein assembly with the BTB-Kelch family of E3 ubiquitin ligases. J. Biol. Chem. *288*, 7803–7814.
22. Spence, H.J., Johnston, I., Ewart, K., Buchanan, S.J., Fitzgerald, U., and Ozanne, B.W. (2000). Krp1, a novel kelch related protein that is involved in pseudopod elongation in transformed cells. Oncogene *19*, 1266–1276.
23. Guerois, R., Nielsen, J.E., and Serrano, L. (2002). Predicting changes in the stability of proteins and protein complexes: a study of more than 1000 mutations. J. Mol. Biol. *320*, 369–387.
24. Lawlor, M.W., Alexander, M.S., Viola, M.G., Meng, H., Joubert, R., Gupta, V., Motohashi, N., Manfready, R.A., Hsu, C.P., Huang, P., et al. (2012). Myotubularin-deficient myoblasts display increased apoptosis, delayed proliferation, and poor cell engraftment. Am. J. Pathol. *181*, 961–968.
25. Kaisto, T., and Metsikkö, K. (2003). Distribution of the endoplasmic reticulum and its relationship with the sarcoplasmic reticulum in skeletal myofibers. Exp. Cell Res. *289*, 47–57.
26. Lu, S., Carroll, S.L., Herrera, A.H., Ozanne, B., and Horowits, R. (2003). New N-RAP-binding partners alpha-actinin, filamin and Krp1 detected by yeast two-hybrid screening: implications for myofibril assembly. J. Cell Sci. *116*, 2169–2178.
27. Paxton, C.W., Cosgrove, R.A., Drozd, A.C., Wiggins, E.L., Woodhouse, S., Watson, R.A., Spence, H.J., Ozanne, B.W., and Pell, J.M. (2011). BTB-Kelch protein Krp1 regulates proliferation and differentiation of myoblasts. Am. J. Physiol. Cell Physiol. *300*, C1345–C1355.
28. Greenberg, C.C., Connelly, P.S., Daniels, M.P., and Horowits, R. (2008). Krp1 (Sarcosin) promotes lateral fusion of myofibril assembly intermediates in cultured mouse cardiomyocytes. Exp. Cell Res. *314*, 1177–1191.
29. Gupta, V., Discenza, M., Guyon, J.R., Kunkel, L.M., and Beggs, A.H. (2012). α-Actinin-2 deficiency results in sarcomeric defects in zebrafish that cannot be rescued by α-actinin-3 revealing functional differences between sarcomeric isoforms. FASEB J. *26*, 1892–1908.
30. Dowling, J.J., Vreede, A.P., Low, S.E., Gibbs, E.M., Kuwada, J.Y., Bonnemann, C.G., and Feldman, E.L. (2009). Loss of myotubularin function results in T-tubule disorganization in zebrafish and human myotubular myopathy. PLoS Genet. *5*, e1000372.
31. Gupta, V.A., Kawahara, G., Myers, J.A., Chen, A.T., Hall, T.E., Manzini, M.C., Currie, P.D., Zhou, Y., Zon, L.I., Kunkel, L.M., and Beggs, A.H. (2012). A splice site mutation in laminin-α2 results in a severe muscular dystrophy and growth abnormalities in zebrafish. PLoS ONE *7*, e43794.
32. Smith, L.S., Beggs, A.H., and Gupta, V.A. (2013). Analysis of skeletal muscle defects in larval zebrafish by birefringence and touch-evoke escape response assays. J. Vis. Exp. *82*, e50925. http://dx.doi.org/10.3791/50925.
33. Zhang, D.D., Lo, S.C., Sun, Z., Habib, G.M., Lieberman, M.W., and Hannink, M. (2005). Ubiquitination of Keap1, a BTB-Kelch substrate adaptor protein for Cul3, targets Keap1 for degradation by a proteasome-independent pathway. J. Biol. Chem. *280*, 30091–30099.
34. Spence, H.J., McGarry, L., Chew, C.S., Carragher, N.O., Scott-Carragher, L.A., Yuan, Z., Croft, D.R., Olson, M.F., Frame, M., and Ozanne, B.W. (2006). AP-1 differentially expressed proteins Krp1 and fibronectin cooperatively enhance Rho-ROCK-independent mesenchymal invasion by altering the function, localization, and activity of nondifferentially expressed proteins. Mol. Cell. Biol. *26*, 1480–1495.

nature genetics

Mutations affecting components of the SWI/SNF complex cause Coffin-Siris syndrome

Yoshinori Tsurusaki[1], Nobuhiko Okamoto[2], Hirofumi Ohashi[3], Tomoki Kosho[4], Yoko Imai[5], Yumiko Hibi-Ko[5], Tadashi Kaname[6], Kenji Naritomi[6], Hiroshi Kawame[7,8], Keiko Wakui[4], Yoshimitsu Fukushima[4], Tomomi Homma[9], Mitsuhiro Kato[10], Yoko Hiraki[11], Takanori Yamagata[12], Shoji Yano[13], Seiji Mizuno[14], Satoru Sakazume[15], Takuma Ishii[15,16], Toshiro Nagai[15], Masaaki Shiina[17], Kazuhiro Ogata[17], Tohru Ohta[18], Norio Niikawa[18], Satoko Miyatake[1], Ippei Okada[1], Takeshi Mizuguchi[1], Hiroshi Doi[1], Hirotomo Saitsu[1], Noriko Miyake[1] & Naomichi Matsumoto[1]

By exome sequencing, we found *de novo SMARCB1* mutations in two of five individuals with typical Coffin-Siris syndrome (CSS), a rare autosomal dominant anomaly syndrome. As *SMARCB1* encodes a subunit of the SWItch/Sucrose NonFermenting (SWI/SNF) complex, we screened 15 other genes encoding subunits of this complex in 23 individuals with CSS. Twenty affected individuals (87%) each had a germline mutation in one of six SWI/SNF subunit genes, including *SMARCB1*, *SMARCA4*, *SMARCA2*, *SMARCE1*, *ARID1A* and *ARID1B*.

Chromatin remodeling factors regulate the gene accessibility and expression by dynamic alteration of chromatin structure. SWI/SNF complexes have important roles in lineage specification, maintenance of stem cell pluripotency and tumorigenesis[1–5]. These complexes are composed of evolutionarily conserved core subunits and variant subunits. Brahma-associated factor (BAF) and Polybromo BAF (PBAF) complexes constitute two major subclasses[1–5]. It has been suggested that the BAF complex is similar to the yeast SWI/SNF complex and that the PBAF complex is more like the chromatin remodelling complex (RSC) in yeast, which is required for cell cycle progression through mitosis[6]. However, several subunits that are common to both BAF and PBAF complexes are predicted to be related to the regulation of lineage- and tissue-specific gene expression[2].

Coffin-Siris syndrome (MIM 135900) is a rare congenital anomaly syndrome characterized by growth deficiency, intellectual disability, microcephaly, coarse facial features and hypoplastic nail of the fifth finger and/or toe (**Fig. 1** and **Supplementary Table 1**)[7]. The majority of affected individuals represent sporadic cases, which is compatible with an autosomal dominant inheritance mechanism. The genetic cause for this syndrome has not been elucidated.

To identify the genetic basis of CSS, we performed whole-exome sequencing of five typical affected individuals (**Supplementary Methods**). Taking into account our model that assumes that an abnormality in a causal gene would be shared in two or more subjects, 51 variants were identified as candidates (**Supplementary Table 2**). All the variants were also examined by Sanger sequencing of PCR products amplified using genomic DNA from the five affected individuals and their parents. Nine variants were found to be false positives, 40 were inherited from either the father or mother, and 2 *de novo* heterozygous mutations of *SMARCB1* were found in 2 affected individuals (c.1130G>A (p.Arg377His) and c.1091_1093del AGA (p.Lys364del)) (**Table 1**, **Supplementary Fig. 1** and **Supplementary Methods**). Two *de novo* coding-sequence mutations occurring within a specific gene is an extremely unlikely event[8], supporting the idea that *SMARCB1* is a causative gene in CSS. Next, we screened *SMARCB1* in 23 individuals with CSS by high-resolution melting analysis[9] and identified the mutation encoding the p.Lys364del alteration in two additional individuals, including one of Arab descent (subject 22) (**Table 1** and **Supplementary Fig. 1**). As the mutation detection rate was relatively low (4 of 23, only 17.4%), we screened 15 additional genes encoding other SWI/SNF subunits (**Supplementary Table 3**). Unexpectedly, four other subunits, *SMARCA4* (also known as *BRG1*), *SMARCE1*, *ARID1A* and *ARID1B* were also found to be mutated (**Table 1** and **Supplementary Figs. 2–5**). In subject 10, a, c.2144C>T mutation in *ARID1B* (encoding p.Pro715Leu) was found in addition to the c.5632delG mutation in *ARID1B*. RT-PCR products that were amplified from total RNA from this subject's lymphoblastoid cells were cloned into the pCR4-TOPO vector. The two mutations were present on different alleles, according to sequencing of clones containing each allele (data not shown). As the c.5632delG mutation is

[1]Department of Human Genetics, Yokohama City University Graduate School of Medicine, Yokohama, Japan. [2]Division of Medical Genetics, Osaka Medical Center and Research Institute for Maternal and Child Health, Izumi, Japan. [3]Division of Medical Genetics, Saitama Children's Medical Center, Iwatsuki, Japan. [4]Department of Medical Genetics, Shinshu University School of Medicine, Matsumoto, Japan. [5]Division of Pediatrics, Japanese Red Cross Medical Center, Tokyo, Japan. [6]Department of Medical Genetics, University of the Ryukyus Faculty of Medicine, Okinawa, Japan. [7]Department of Genetic Counseling, Graduate School of Humanities and Sciences, Ochanomizu University, Tokyo, Japan. [8]Division of Medical Genetics, Nagano Children's Hospital, Azumino, Japan. [9]Division of Pediatrics, Yamagata Prefectural and Sakata Municipal Hospital Organization, Nihonkai General Hospital, Sakata, Japan. [10]Department of Pediatrics, Yamagata University Faculty of Medicine, Yamagata, Japan. [11]Hiroshima Municipal Center for Child Health and Development, Hiroshima, Japan. [12]Department of Pediatrics, Jichi Medical University, Tochigi, Japan. [13]Genetics Division, Department of Pediatrics, Los Angeles County and University of Southern California Medical Center, Keck School of Medicine, University of Southern California, Los Angeles, California, USA. [14]Department of Pediatrics, Central Hospital, Aichi Human Service Center, Kasugai, Japan. [15]Department of Pediatrics, Koshigaya Hospital, Dokkyo University School of Medicine, Koshigaya, Japan. [16]Nakagawa-No-Sato, Hospital for the Disabled, Saitama, Japan. [17]Department of Biochemistry, Yokohama City University Graduate School of Medicine, Yokohama, Japan. [18]Research Institute of Personalized Health Sciences, Health Sciences University of Hokkaido, Ishikari-Tobetsu, Japan. Correspondence should be addressed to N. Matsumoto (naomat@yokohama-cu.ac.jp) or N. Miyake (nmiyake@yokohama-cu.ac.jp).

Received 29 September 2011; accepted 10 February 2012; published online 18 March 2012; doi:10.1038/ng.2219

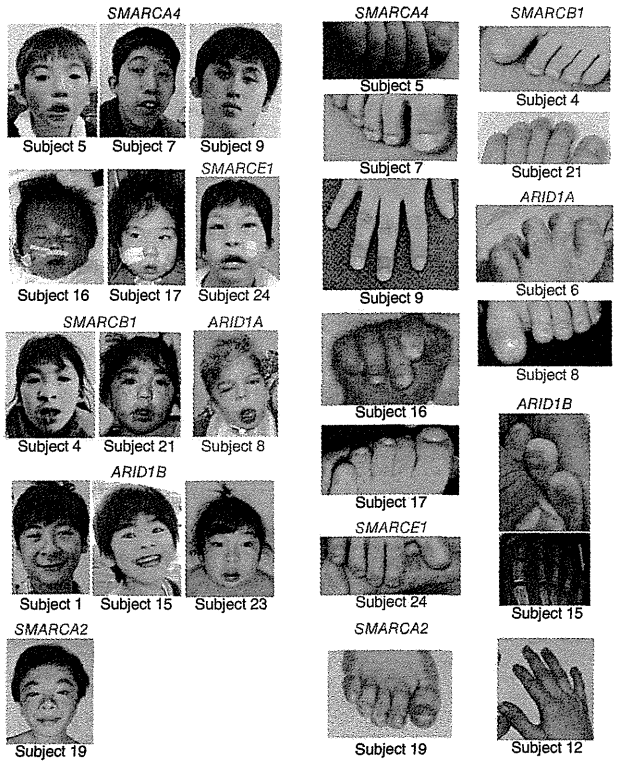

Figure 1 Photographs of individuals with Coffin-Siris syndrome. The faces (left) and hypoplastic-to-absent nail of the fifth finger or toe (right) of affected individuals are shown with the color-coded names of the corresponding mutated genes. The green arrow indicates the absence of the distal phalanx in the fifth toe. No obvious hypoplastic nails were observed in subjects 12 or 19. Consent for all the photographs was obtained from the families of the affected individuals.

very likely to be deleterious (as it results in a truncated protein), the c.2144C>T mutation is likely to be a rare polymorphism. Of note, subject 12, who presented an atypical facial appearance and indistinct hypoplastic nails, had two interstitial deletions at 6q25.3–q27 involving *ARID1B*, as detected by a SNP array (**Supplementary Fig. 6** and **Supplementary Methods**). Furthermore, subject 14 was found to have an interstitial deletion of *SMARCA2* by a SNP array (**Supplementary Fig. 7** and **Supplementary Methods**). No other copy-number changes involving genes encoding SWI/SNF complex components were found in subjects 2, 14 or 18 by array analysis. The overall mutation detection rate was 87%. In total, 20 of the 23 subjects had a mutation affecting one of the six SWI/SNF subunits.

Mutations in CSS were identified in the BAF-specific subunits *ARID1A* and *ARID1B* but not in PBAF-specific subunits (*BRD7*, *ARID2* and *PBRM1*) (**Supplementary Table 3**). In addition, mutations were identified in *SMARCA4* (*BRG1*) as well as in *SMARCA2* (*BRM*) (**Supplementary Table 3**). The BRG1 and BRM proteins are mutually exclusive catalytic ATP subunits in mammalian SWI/SNF complexes. Of note, the majority of heterozygous *Smarca4*-null mice survive with susceptibility to neoplasia, with a minority dying after birth because of exencephaly, whereas homozygous *Smarca2*-null mice are viable and fertile[4]. In *Smarca2*-null mice, Brg1 is upregulated, suggesting that Brg1 can functionally replace Brm in mice[10]. However, in humans, abnormalities in both *SMARCA4* and *SMARCA2* are found in CSS, indicating that the in-frame partial deletion of the gene encoding BRM in subject 19 has a specific mutational effect different from that of simple inactivation in mice. These data support the idea that abnormalities in the BRG1-BAF and BRM-BAF complexes can cause the abnormal neurological development in CSS.

All the mutated genes found in CSS, except for *SMARCE1*, have been reported to be associated with tumorigenesis[1,2]. Among the 23 subjects with CSS, only subject 3 with an *ARID1A* mutation presented with hepatoblastoma. To our knowledge, haploinsufficiency and/or homozygous inactivation of *ARID1A* have been found in several types of cancer but not in hepatoblastoma. Malignancies were not detected in any of the other subjects with CSS examined here. It remains to be seen whether malignancies are robustly associated with CSS.

Given the fact that all the mutations in *ARID1A* and *ARID1B* in CSS were predicted to cause protein truncation, we proposed that haploinsufficiency of these two genes must be able to cause CSS. cDNA analysis of lymphoblastoid cell lines from subjects 1, 6 and 23 indicated that the mutated transcripts were subject to nonsense-mediated mRNA decay (**Supplementary Fig. 8**). In subject 10, the *ARID1B* mutation associated with the creation of a premature stop codon in the last exon did not result in nonsense-mediated mRNA decay as expected (**Supplementary Fig. 8**).

In regard to the other mutated genes, germline heterozygous truncation mutations in *SMARCB1* and *SMARCA4* have been reported

Table 1 Mutations in individuals with Coffin-Siris syndrome

Subject ID	Gene	Mutation	Alteration	Type	Control allele frequency[a]
4	*SMARCB1*	c.1091_1093del AGA	p.Lys364del	*De novo*	0/502
11	*SMARCB1*	c.1130G>A	p.Arg377His	*De novo*	0/500
21	*SMARCB1*	c.1091_1093del AGA	p.Lys364del	NC	0/502
22	*SMARCB1*	c.1091_1093del AGA	p.Lys364del	NC	0/502
9	*SMARCA4*	c.1636_1638del AAG	p.Lys546del	*De novo*	0/350
7	*SMARCA4*	c.2576C>T	p.Thr859Met	*De novo*	0/368
5	*SMARCA4*	c.2653C>T	p.Arg885Cys	*De novo*	0/368
16	*SMARCA4*	c.2761C>T	p.Leu921Phe	*De novo*	0/368
25	*SMARCA4*	c.3032T>C	p.Met1011Thr	NC	0/372
17	*SMARCA4*	c.3469C>G	p.Arg1157Gly	*De novo*	0/368
19	*SMARCA2*	Partial deletion		*De novo*	–
24	*SMARCE1*	c.218A>G	p.Tyr73Cys	*De novo*	0/368
3	*ARID1A*	c.31_56del	p.Ser11Alafs*91	NC	0/330
6	*ARID1A*	c.2758C>T	p.Gln920*	NC	0/376
8	*ARID1A*	c.4003C>T	p.Arg1335*	*De novo*	–
1	*ARID1B*	c.1678_1688del	p.Ile560Glyfs*89	*De novo*	–
15	*ARID1B*	c.1903C>T	p.Gln635*	*De novo*	–
23	*ARID1B*	c.3304C>T	p.Arg1102*	*De novo*	–
10	*ARID1B*	c.2144C>T	p.Pro715Leu	NC	0/368
10	*ARID1B*	c.5632del G	p.Asp1878Metfs*96	NC	0/374
12	*ARID1B*	Microdeletion		NC	–

NC, not confirmed because parental samples were unavailable.
[a]The numbers indicate the observed allele frequency (alleles harboring the change/total tested alleles) in Japanese controls. None of the mutations was found in dbSNP132, the 1000 Genomes database or the National Heart, Lung, and Blood Institute (NHLBI) GO exomesequencing project database. –, not tested.

in individuals with rhabdoid tumor predisposition syndromes 1 (RTPS1; MIM 609322) and 2 (RTPS2; MIM 613325)[11,12], and various types of *SMARCB1* mutations (missense, in-frame deletion, nonsense and splice site) have been found in the germline of individuals with familial and sporadic schwannomatosis (MIM 162091)[13,14]. Furthermore, mice with heterozygous knockout of *Smarca4* or *Smarcb1* were prone to tumor development[2]. All the mutations in *SMARCA4* and *SMARCB1* in individuals with CSS were nontruncating (either missense or in-frame deletions), implying that they exert gain-of-function or dominant-negative effects (excluding haploinsufficiency as a cause). It is noteworthy that comparable germline mutations in *SMARCB1* have such different phenotypic consequences in their association with the phenotypes of CSS and schwannomatosis. The *SMARCB1* mutations in CSS and those in schwannomatosis are indeed different according to the Human Gene Mutation Database. With regard to the *SMARCA2* interstitial deletion in CSS, the change maintained the coding sequence reading frame but removed exons 20–27 that encode the HELICc domain. RT-PCR analysis confirmed the deletion of exons 20–27 at the cDNA level (**Supplementary Fig.** 7). These data suggest the importance of the HELICc domain in the SMARCA2 protein.

The various types of mutations in the genes encoding different SWI/SNF components resulted in similar CSS phenotypes. This suggests that the SWI/SNF complexes coordinately regulate chromatin structure and gene expression. This is the first report, to our knowledge, of germline mutations in SWI/SNF complex genes associated with a multiple congenital anomaly syndrome, highlighting new biological aspects of SWI/SNF complexes in humans. Similarly, genes encoding SNF2-related proteins, which are implicated as chromatin remodeling factors outside of SWI/SNF complexes, are mutated in different syndromes, including in α-thalassaemia/mental retardation syndrome X-linked (ATRX; *ATRX* mutations) and in coloboma, heart defect, atresia choanae, retarded growth and development, genital abnormality and ear abnormality (CHARGE) syndrome (*CHD7* haploinsufficiency)[3]. We expect that more mutations affecting chromatin remodeling factors will be found in different human diseases.

URLs. Human Gene Mutation Database, https://portal.biobase-international.com/cgi-bin/portal/login.cgi.

Note: Supplementary information is available on the Nature Genetics website.

ACKNOWLEDGMENTS

We thank all the family members for participating in this study. This work was supported by research grants from the Ministry of Health, Labour and Welfare (to N. Miyake, H.S. and N. Matsumoto), the Japan Science and Technology Agency (to N. Matsumoto), the Strategic Research Program for Brain Sciences (to N. Matsumoto), the Japan Epilepsy Research Foundation (to H.S.) and the Takeda Science Foundation (to N. Matsumoto and N. Miyake). This study was also funded by a Grant-in-Aid for Scientific Research on Innovative Areas (Foundation of Synapse and Neurocircuit Pathology) from the Ministry of Education, Culture, Sports, Science and Technology of Japan (to N. Matsumoto), a Grant-in-Aid for Scientific Research from the Japan Society for the Promotion of Science (to N. Matsumoto), a Grant-in-Aid for Young Scientists from the Japan Society for the Promotion of Science (to N. Miyake and H.S.) and a Grant for 2011 Strategic Research Promotion of Yokohama City University (to N. Matsumoto). This study was performed at the Advanced Medical Research Center at Yokohama City University. Informed consent was obtained from all the families of affected individuals. The Institutional Review Board of Yokohama City University approved this study.

AUTHOR CONTRIBUTIONS

Y.T., S. Miyatake, I.O., H.D., H.S. and N. Miyake performed exome sequencing and Sanger sequencing. Y.T., M.S., K.O., I.O., T.M., H.D., H.S. and N. Miyake performed data management and analysis. N.O., H.O., T. Kosho, Y.I., Y.H.-K., T. Kaname, K.N., H.K., K.W., Y.F., T.H., M.K., Y.H., T.Y., S.Y., S. Mizuno, S.S., T.I., T.N., T.O. and N.N. provided clinical materials after careful evaluation. Y.T., N. Miyake and N. Matsumoto wrote the manuscript. N. Matsumoto designed and oversaw all aspects of the study.

COMPETING FINANCIAL INTERESTS

The authors declare no competing financial interests.

Published online at http://www.nature.com/naturegenetics/.
Reprints and permissions information is available online at http://www.nature.com/reprints/index.html.

1. Reisman, D., Glaros, S. & Thompson, E.A. *Oncogene* **28**, 1653–1668 (2009).
2. Wilson, B.G. & Roberts, C.W. *Nat. Rev. Cancer* **11**, 481–492 (2011).
3. Clapier, C.R. & Cairns, B.R. *Annu. Rev. Biochem.* **78**, 273–304 (2009).
4. Bultman, S. *et al. Mol. Cell* **6**, 1287–1295 (2000).
5. Hargreaves, D.C. & Crabtree, G.R. *Cell Res.* **21**, 396–420 (2011).
6. Xue, Y. *et al. Proc. Natl. Acad. Sci. USA* **97**, 13015–13020 (2000).
7. Coffin, G.S. & Siris, E. *Am. J. Dis. Child.* **119**, 433–439 (1970).
8. Bamshad, M.J. *et al. Nat. Rev. Genet.* **12**, 745–755 (2011).
9. Wittwer, C.T., Reed, G.H., Gundry, C.N., Vandersteen, J.G. & Pryor, R.J. *Clin. Chem.* **49**, 853–860 (2003).
10. Reyes, J.C. *et al. EMBO J.* **17**, 6979–6991 (1998).
11. Schneppenheim, R. *et al. Am. J. Hum. Genet.* **86**, 279–284 (2010).
12. Taylor, M.D. *et al. Am. J. Hum. Genet.* **66**, 1403–1406 (2000).
13. Boyd, C. *et al. Clin. Genet.* **74**, 358–366 (2008).
14. Hadfield, K.D. *et al. J. Med. Genet.* **45**, 332–339 (2008).

Reply

Aron S. Buchman, MD,[1,2] Joshua M. Shulman, MD, PhD,[3,4] Sue E. Leurgans, PhD,[1,2] Julie A. Schneider, MD, MS,[1,2,5] and David A. Bennett, MD[1,2]

We thank Drs Jellinger and Attems for their interest in our study. In agreement with prior reports, we found that Parkinson disease (PD) pathology, including nigral neuronal loss and Lewy body pathology, is common in older adults without PD. Furthermore, we provide evidence that PD nigral pathology is related to parkinsonian motor signs in persons without a clinical diagnosis of PD.[1] This contrasts with prior studies of incidental Lewy body disease, which found associations with subtle electrophysiologic changes but not with overt motor signs.[2] Interestingly, in the current study, we also found that Alzheimer disease (AD) and cerebrovascular pathology showed independent associations with the severity of parkinsonian motor signs.[1] As requested, the correlations among these common brain pathologies are included in the accompanying Table. It is interesting that Dr Attems and colleagues did not find an association of nigral pathology or cerebrovascular disease with parkinsonian signs among persons with AD.[3] We and others have reported such associations.[4–6] Overall, the findings in the current study have important public health implications. They suggest that mild parkinsonian signs, reported in up to 50% of older adults by age 85 years and associated with significant morbidity and mortality, may be caused by a range of pathologies including PD pathology, AD, and cerebrovascular pathologies. These data underscore the need for more sensitive clinical measures and biomarkers that can detect and differentiate the various neuropathologies underlying the development of parkinsonian signs in old age.

Potential Conflicts of Interest

Nothing to report.

[1]Rush Alzheimer's Disease Center and [2]Department of Neurological Sciences, Rush University Medical Center, Chicago, IL, [3]Department of Neurology, Brigham and Women's Hospital, Boston, MA, [4]Department of Neurology, Harvard Medical School, Boston, MA, and [5]Department of Pathology (Neuropathology), Rush University Medical Center, Chicago, IL

References

1. Buchman AS, Shulman JM, Nag S, et al. Nigral pathology and parkinsonian signs in elders without Parkinson disease. Ann Neurol 2012;71:258–266.
2. Caviness JN. Presymptomatic Parkinson's disease: the Arizona experience. Parkinsonism Relat Disord 2012;18(suppl 1):S203–S206.
3. Attems J, Quass M, Jellinger K. Tau and α-synuclein brainstem pathology in Alzheimer disease: relation with extrapyramidal signs. Acta Neuropathol 2007;113:53–62.
4. Burns JM, Galvin JE, Roe CM, et al. The pathology of the substantia nigra in Alzheimer disease with extrapyramidal signs. Neurology 2005;64:1397–1403.
5. Schneider JA, Li JL, Li Y, et al. Substantia nigra tangles are related to gait impairment in older persons. Ann Neurol 2006;59:166–173.
6. Buchman AS, Leurgans SE, Nag S, et al. Cerebrovascular disease pathology and parkinsonian signs in old age. Stroke 2011;42:3183–3189.

DOI: 10.1002/ana.23639

Whole Exome Sequencing Identifies *KCNQ2* Mutations in Ohtahara Syndrome

Hirotomo Saitsu, MD, PhD,[1] Mitsuhiro Kato, MD, PhD,[2] Ayaka Koide, MD, PhD,[3] Tomohide Goto, MD, PhD,[3] Takako Fujita, MD,[4] Kiyomi Nishiyama, PhD,[1] Yoshinori Tsurusaki, PhD,[1] Hiroshi Doi, MD, PhD,[1] Noriko Miyake, MD, PhD,[1] Kiyoshi Hayasaka, MD, PhD,[2] and Naomichi Matsumoto, MD, PhD[1]

Recently, Weckhuysen et al revealed that *KCNQ2* mutations are involved in a substantial proportion of patients with a neonatal epileptic encephalopathy.[1] Some cases showed a suppression–burst pattern on electroencephalogram (EEG), tonic seizures, and profound intellectual disability, resembling Ohtahara syndrome (OS). By whole exome sequencing analysis of 12

TABLE: Intercorrelation of Postmortem Indices

Index	Macroinfarcts	Microinfarcts	Arteriolosclerosis	AD Pathology	Nigral Lewy Bodies
Nigral neuronal loss	0.07, 0.068	0.02, 0.628	0.13, <0.001	0.14, <0.001	0.38, <0.001
Macroinfarcts	—	0.39, 0.056	0.26, <0.001	0.09, 0.017	−0.063, 0.072
Microinfarcts		—	0.15, <0.001	0.04, 0.315	−0.10, 0.075
Arteriolosclerosis			—	0.03, 0.385	0.03, 0.491
AD pathology				—	0.07, 0.052

Based on Spearman or tetrachoric correlation and *p* value.

TABLE: Summary of the Clinical Features of Subjects with *KCNQ2* Mutations

Case #	Mutation	Sex	Age	Age at Onset, Days	Initial Symptoms	Initial Epileptic Attacks	Initial EEG	Age at Onset of Spasms, Days	Age at Onset of SB Pattern, Days	Response to Therapy	Other Drugs Used, but Ineffective	Development	Neurological Examination	Involuntary Movement
1469	c.1010C>G (p.A337G) de novo	M	7 years	7	Vomiting	7 days, tonic seizure	SB	—	22	Seizure free and SB on EEG, disappeared after high-dose PB, CPS since age 5 years	B6, ZNS	No meaningful words, able to crawl, stand with support	Severe MR, no pyramidal signs	No
1654	c.341C>T (p.T114I) de novo	F	7 years	0	Tremor of the upper extremities	2 days, generalized convulsion with cyanosis	SB	—	2	Seizure free after ZNS, CPS since age 5 years	B6, CZP, PHT	DQ 10, bed-ridden, smiling	Profound MR, spastic quadriplegia	No
1754	c.794C>T (p.A265V) de novo	M	3 months	1	Apneic spell	1 days, tonic spasms with right opsoclonuslike movement	SB	1	2	Intractable	B6, ZNS, VPA, CZP, CBZ	Delayed, no eye pursuit	Unknown	Myoclonus at the bilateral upper extremities

B6 = vitamin B6; CBZ = carbamazepine; CPS = complex partial seizures; CZP = clonazepam; DQ = developmental quotient; EEG = electroencephalogram; MR = mental retardation; PB = phenobarbital; PHT = phenytoin; SB = suppression–burst; VPA = valproic acid; ZNS = zonisamide.

patients with OS, we found 3 missense mutations in *KCNQ2* (25%): c.341C>T (p.T114I), c.1010C>G (p.A337G), and c.794C>T (p.A265V) in 3 patients. All 3 patients showed initial seizures early in the neonatal period and a characteristic suppression–burst pattern on EEG, leading to diagnosis as OS (Table). Seizures were temporarily well controlled in 2 patients. Consistent with Weckhuysen's report, in which 6 of 8 mutations arose de novo, the 3 mutations in our series are de novo changes. Thus, it is likely that de novo *KCNQ2* mutations are among the common causes of early onset epileptic encephalopathies, including OS. *KCNQ2* mutations have been shown to cause benign familial neonatal seizures, which is distinct from OS.[2,3] We unexpectedly found *KCNQ2* mutations by whole exome sequencing. Exome sequencing using familial trios (patients and their parents) can identify de novo mutations.[4] Novel associations between unexpected gene mutations and early onset epileptic encephalopathies may be validated by such new technologies.

Acknowledgment

Supported by a research grant from the Ministry of Health, Labor, and Welfare, Japan (H.S., M.K., N.Mi., N.Ma.), a Grant-in-Aid for Scientific Research from the Japan Society for the Promotion of Science (H.S., M.K., N.Mi., N.Ma.), a research grant from the Japan Science and Technology Agency (N.Ma.), and the Strategic Research Program for Brain Sciences (a Grant-in-Aid for Scientific Research on Innovative Areas, Foundation of Synapse and Neurocircuit Pathology; N.Ma.).

Potential Conflicts of Interest

Nothing to report.

[1]Department of Human Genetics, Yokohama City University Graduate School of Medicine, Yokohama, [2]Department of Pediatrics, Yamagata University Faculty of Medicine, Yamagata, [3]Department of Neurology, Tokyo Metropolitan Children's Medical Center, Fuchu, and [4]Department of Pediatrics, Fukuoka University Faculty of Medicine, Fukuoka, Japan

References

1. Weckhuysen S, Mandelstam S, Suls A, et al. KCNQ2 encephalopathy: emerging phenotype of a neonatal epileptic encephalopathy. Ann Neurol 2012;71:15–25.
2. Singh NA, Charlier C, Stauffer D, et al. A novel potassium channel gene, KCNQ2, is mutated in an inherited epilepsy of newborns. Nat Genet 1998;18:25–29.

3. Biervert C, Schroeder BC, Kubisch C, et al. A potassium channel mutation in neonatal human epilepsy. Science 1998;279: 403–406.

4. Vissers LE, de Ligt J, Gilissen C, et al. A de novo paradigm for mental retardation. Nat Genet 2010;42:1109–1112.

DOI: 10.1002/ana.23620

Brain Death in Children: Why Does It Have to Be So Complicated?

Thomas Nakagawa, MD,[1] Stephen Ashwal, MD,[2] Mudit Mathur, MD,[3] and Mohan Mysore, MD[4]

The authors appreciate the editorial comments by Wijdicks and Smith[1] and would like to address concerns about why the diagnosis of brain death in pediatric patients has to be "so complicated."

This revised clinical guideline focused specifically on determining brain death and deliberately excluded issues related to ethical concerns and organ donation. Failure to mention the Child Neurology Society (CNS) as the third sponsoring society of this guideline is a major oversight of the editorial.[1] CNS provided significant review by Practice Committee members and the society's Executive Board.[2] The quality of evidence provided in this guideline was equivalent to, if not more comprehensive than, the revised American Academy of Neurology (AAN) guideline, which reported only class III or IV evidence for 4 of 5 questions posed.[3] We used the GRADE system to develop a consensus guideline because no class I or II studies to determine pediatric brain death exist.[2] Interestingly, the AAN is currently revising guideline development for practicing neurologists to use a modification of the GRADE system.

A wide range of clinical entities can result in brain death in newborns, children, and adolescents. The guideline, the checklist, and Table 3 clearly state that all reversible conditions should be excluded prior to the first brain death examination. However, some uncertainty in the newborn period still exists leading to age-based observation periods. These consensus based recommendations reflect extensive clinical experience across several pediatric disciplines. Additionally, provisions for pediatric trauma patients and neonates were included. Virtually every committee member has cared for acutely injured children who met examination criteria for brain death within the initial 24 hours. Some recovered brain function although most did not which is why 2 examinations over defined time periods is recommended. The recommended time periods are consensus based rather than arbitrary time periods. Neurologic examination findings remaining unchanged and consistent with brain death throughout the observation period was one of the recommended criteria for determining brain death in the 1987 guidelines. The committee retained this recommendation in the current update. We agree that apparent neurologic improvements reported in anecdotal cases are due to diagnostic errors when critically examined; this is precisely the reason why a change in findings between examinations implies the neurological process is potentially reversible, precluding the diagnosis of brain death.

The revised guideline repeatedly states that brain death is a clinical diagnosis, and factors influencing the neurologic examination must be corrected before initiating brain death evaluation and apnea testing. Ancillary studies do not trump the neurological examination, and we clearly state that ancillary studies should not be viewed as a substitute for the neurologic examination. However, situations exist where ancillary studies are helpful to determine death. The revised guideline and checklist have simplified and clarified many previous sources of confusion. Additionally, the checklist will help standardize determination and documentation of brain death in children.[4]

Prolonging declaration of death does not appear to be a major concern in children—perhaps differing from the experience in adults. Families appreciate the added certainty conferred by the second examination. Patients in children's hospitals rely on assessments by pediatric specialists who understand the unique needs of children and their families. The approach to caring for children is very different and likely more family centered. These issues are further addressed in the full guideline and we encourage readers to review the entire document published in Critical Care Medicine and Pediatrics.[2,5]

Declaring brain death in children is complicated and should be undertaken by physicians who are adequately trained in the complexities involved in this important determination. We agree more research is needed to address some of the other issues raised in the editorial, and we again thank Drs Wijdicks and Smith for their opinion.

Potential Conflicts of Interest

Nothing to report.

[1]Departments of Anesthesiology (Section on Pediatric Critical Care) and Pediatrics, Wake Forest School of Medicine, Winston-Salem, NC, [2]Department of Pediatrics (Division of Child Neurology) and [3]Division of Pediatric Critical Care, Loma Linda University School of Medicine, Loma Linda, CA, and [4]Department of Pediatrics, University of Nebraska College of Medicine, Omaha, NE

References

1. Wijdicks EF, Smith WS. Brain death in children: why does it have to be so complicated? Ann Neurol 2012;71:442–443.

2. Nakagawa TA, Ashwal S, Mathur M, et al. Guidelines for the determination of brain death in infants and children: an update of the 1987 Task Force recommendations. Crit Care Med 2011;39:2139–2155.

3. Wijdicks EF, Varelas PN, Gronseth GS, et al. Evidence-based guideline update: determining brain death in adults: report of the Quality Standards Subcommittee of the American Academy of Neurology. Neurology 2010;74:1911–1918.

4. Fackler J, Goldstein B. Pediatric brain death. Crit Care Med 2011; 39;2197–2198.

5. Clinical report - Guidelines for the Determination of Brain Death in Infants and Children. An Update of the 1987 Task Force Recommendations. Nakagawa TA, Ashwal, SA, Mathur M, Mysore M., and the Committee for Brain Death in Infants and Children. Pediatrics. 2011;128:3 e720-e740. doi: 10.1542/peds.2011-1511.

DOI: 10.1002/ana.23623

REPORT

Mutations in *POLR3A* and *POLR3B* Encoding RNA Polymerase III Subunits Cause an Autosomal-Recessive Hypomyelinating Leukoencephalopathy

Hirotomo Saitsu,[1,*] Hitoshi Osaka,[2] Masayuki Sasaki,[3] Jun-ichi Takanashi,[4] Keisuke Hamada,[5] Akio Yamashita,[6] Hidehiro Shibayama,[7] Masaaki Shiina,[5] Yukiko Kondo,[1] Kiyomi Nishiyama,[1] Yoshinori Tsurusaki,[1] Noriko Miyake,[1] Hiroshi Doi,[1] Kazuhiro Ogata,[5] Ken Inoue,[8] and Naomichi Matsumoto[1,*]

Congenital hypomyelinating disorders are a heterogeneous group of inherited leukoencephalopathies characterized by abnormal myelin formation. We have recently reported a hypomyelinating syndrome characterized by diffuse cerebral hypomyelination with cerebellar atrophy and hypoplasia of the corpus callosum (HCAHC). We performed whole-exome sequencing of three unrelated individuals with HCAHC and identified compound heterozygous mutations in *POLR3B* in two individuals. The mutations include a nonsense mutation, a splice-site mutation, and two missense mutations at evolutionally conserved amino acids. Using reverse transcription-PCR and sequencing, we demonstrated that the splice-site mutation caused deletion of exon 18 from *POLR3B* mRNA and that the transcript harboring the nonsense mutation underwent nonsense-mediated mRNA decay. We also identified compound heterozygous missense mutations in *POLR3A* in the remaining individual. *POLR3A* and *POLR3B* encode the largest and second largest subunits of RNA Polymerase III (Pol III), RPC1 and RPC2, respectively. RPC1 and RPC2 together form the active center of the polymerase and contribute to the catalytic activity of the polymerase. Pol III is involved in the transcription of small noncoding RNAs, such as 5S ribosomal RNA and all transfer RNAs (tRNA). We hypothesize that perturbation of Pol III target transcription, especially of tRNAs, could be a common pathological mechanism underlying *POLR3A* and *POLR3B* mutations.

Congenital hypomyelinating disorders form a heterogeneous group of central nervous system leukoencephalopathies that is characterized by abnormal myelin formation. Although these conditions are readily recognized by brain magnetic resonance imaging (MRI), many cases are not diagnosed correctly.[1] Several syndromes affecting myelination, such as hypomyelination with hypodontia and hypogonadotropic hypogonadism (4H) syndrome (MIM 612440) and hypomyelination with atrophy of the basal ganglia and cerebellum (H-ABC) (MIM 612438), have been described.[2–5] We have recently reported a hypomyelinating syndrome characterized by diffuse cerebral hypomyelination with cerebellar atrophy and hypoplasia of the corpus callosum (HCAHC).[6] Individuals with HCAHC do not show hypodontia or atrophy of the basal ganglia, which are observed in 4H syndrome and H-ABC; however, diffuse hypomyelination, atrophy, or hypoplasia of the cerebellum and corpus callosum are overlapping features of these three syndromes, suggesting that there might be a common underlying pathological mechanism.

Here, we report on four individuals with HCAHC from three unrelated families (Figure 1A; Table 1). Clinical information and peripheral blood or saliva samples were obtained from the family members after obtaining written informed consent. Experimental protocols were approved by the Institutional Review Board of Yokohama City University. To identify pathogenic mutations, we performed whole-exome sequencing of three probands from three unrelated families (individuals 1, 3, and 4). DNAs were captured with the SureSelect Human All Exon 50Mb Kit (Agilent Technologies, Santa Clara, CA) and sequenced with one lane per sample on an Illumina GAIIx (Illumina, San Diego, CA) with 108 bp paired-end reads. Image analysis and base calling were performed by sequence control software real-time analysis and CASAVA software v1.7 (Illumina). A total of 90,014,368 (individual 1), 86,942,264 (individual 3), and 92,168,758 (individual 4) paired-end reads were obtained and aligned to the human reference genome sequence (GRCh37/hg19) with MAQ[7] and NextGENe software v2.00 with sequence condensation by consolidation (SoftGenetics, State College, PA). This approach resulted in more than 88% of target exomes being covered by ten reads or more (see Table S1, available online). Single nucleotide variants (SNVs) were called with MAQ and NextGENe. Small insertions and deletions were

[1]Department of Human Genetics, Yokohama City University Graduate School of Medicine, 3-9 Fukuura, Kanazawa-ku, Yokohama 236-0004, Japan; [2]Division of Neurology, Clinical Research Institute, Kanagawa Children's Medical Center, 2-138-4 Mutsukawa, Minami-ku, Yokohama 232-8555, Japan; [3]Department of Child Neurology, National Center of Neurology and Psychiatry, 4-1-1 Ogawahigashi-cho Kodaira, Tokyo 187-8551, Japan; [4]Department of Pediatrics, Kameda Medical Center, 929 Higashi-cho, Kamogawa-shi, Chiba 296-8602, Japan; [5]Department of Biochemistry, Yokohama City University Graduate School of Medicine, 3-9 Fukuura, Kanazawa-ku, Yokohama 236-0004, Japan; [6]Department of Molecular Biology, Yokohama City University Graduate School of Medicine, 3-9 Fukuura, Kanazawa-ku, Yokohama 236-0004, Japan; [7]Department of Neurology, Kameda Medical Center, 929 Higashi-cho, Kamogawa-shi, Chiba 296-8602, Japan; [8]Department of Mental Retardation and Birth Defect Research, National Institute of Neuroscience, National Center of Neurology and Psychiatry, 4-1-1 Ogawahigashi-cho Kodaira, Tokyo 187-8551, Japan
*Correspondence: hsaitsu@yokohama-cu.ac.jp (H.S.), naomat@yokohama-cu.ac.jp (N.M.)
DOI 10.1016/j.ajhg.2011.10.003.

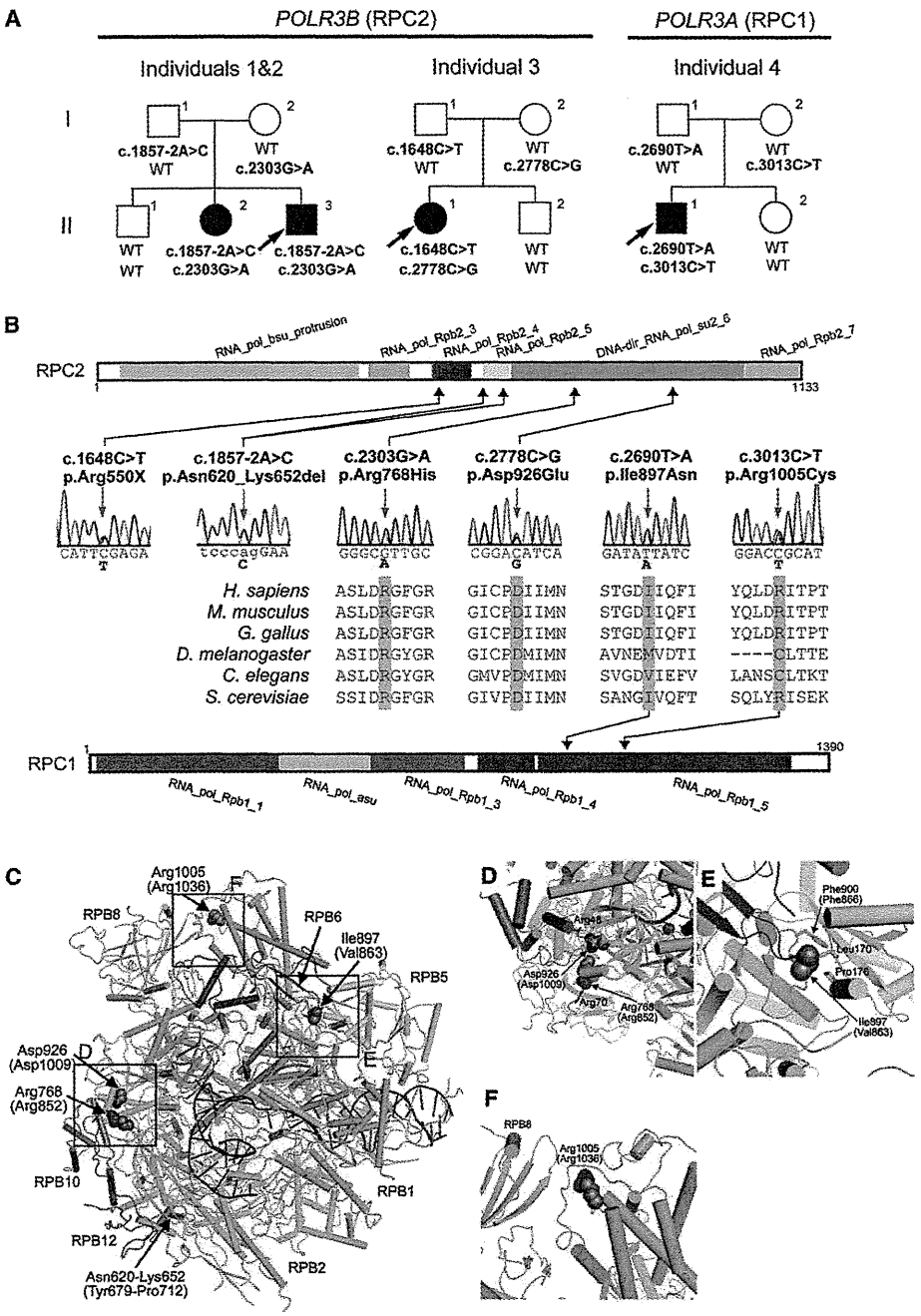

Figure 1. Mutations in *POLR3B* and *POLR3A*

(A) Pedigrees of four kindreds with HCAHC are shown. We identified four mutations in *POLR3B* encoding RPC2 in three individuals from two unrelated families and two mutations in *POLR3A* encoding RPC1 in one family. The segregation of each mutation is shown.

(B) Schematic representation of RPC2 (upper) and RPC1 (lower) proteins with Pfam domains (from Ensembl). Locations of each amino-acid-altering mutation are depicted with electropherograms. All of the missense mutations occurred at evolutionally conserved amino acids. Homologous sequences were aligned with the CLUSTALW website.

(C–F) 3D representations of RPC1 and RPC2 mutations. Mutated amino acids in RPC1 and RPC2 are shown along with their equivalent positions in the homologous RPB1 and RPB2 subunits of RNA Polymerase II (amino acid and its position in parenthesis). The structure and positions of mutations are illustrated by PyMOL with the crystal structure (PDB accession number 3GTP). RPB3, RPB9, and RPB11 subunits, which are specific to RNA Polymerase II, have been omitted from the figure. RPB1 is shown in green, RPB2 in sky blue, RPB5 in yellow, RPB6 in dark blue, RPB8 in pink, RPB10 in orange, RPB12 in purple, DNA in brown, and RNA in red. Amino acids that interact with mutated amino acids are also shown.

Table 1. Clinical Features of the Individuals

Clinical Features	Individual 1	Individual 2	Individual 3	Individual 4
Genes	*POLR3B*	*POLR3B*	*POLR3B*	*POLR3A*
Mutations, DNA	c.1857-2A>C, c.2303G>A	c.1857-2A>C, c.2303G>A	c.1648C>T, c.2778C>G	c.2690T>A, c.3013C>T
Mutations, protein	p.Asn620_Lys652del, p.Arg768His	p.Asn620_Lys652del, p.Arg768His	p.Arg550X, p.Asp926Glu	p.Ile897Asn, p.Arg1005Cys
Gender	M	F	F	M
Current age (years)	27	30	16	17
Intellectual disability	mild	mild	moderate	mild
Cognitive regression	–	–	–	–
Seizures	–	–	–	–
Initial motor development	normal	normal	normal	normal
Age of onset (years)	3	3	2	4
Motor deterioration	–	–	–	+
Wheelchair use	–	–	–	+
Optic atrophy	–	–	–	–
Myopia	+	+	–	+
Nystagmus	+	+	–	–
Abnormal pursuit	+	+	+	–
Vertical gaze limitation	+	+	+	–
Dysphagia	–	–	+	–
Hypersalivation	–	–	–	–
Cerebellar signs	+	+	+	+
Tremor	–	+	+	+
Babinski refex	–	–	–	–
Spasticity	–	–	mild	–
Peripheral nerve involvement	–	–	–	–
Nerve biopsy	NA	NA	NA	NA
Hypodontia	–	–	–	–
Hypogonadism	+	+	–	–

NA is an abbreviation for not available.

detected with NextGENe. Called SNVs were annotated with SeattleSeq Annotation.

We adopted a prioritization scheme to identify the pathogenic mutation in each individual, similar to the approach taken by recent studies (Table S2).[8–10] First, we excluded the variants registered in the dbSNP131 or 1000 Genome Project from all the detected variants. Then, SNVs commonly detected by MAQ and NextGENe analyses were selected as highly confident variants; 364 to 374 SNVs of nonsynonymous (NS) or canonical splice-site (SP) changes, along with 113 to 124 small insertions or deletions (indels), were identified per individual. We also excluded variants found in our 55 in-house exomes, which are derived from 12 healthy individuals and 43 individuals with unrelated diseases, reducing the number of candidate variants to ~250 per individual. Assuming that HCAHC is an autosomal-recessive disorder based on two affected individuals in one pedigree (individuals 1 and 2), we focused on rare heterozygous variants that are not registered in the dbSNP or in our in-house 55 exomes.

We surveyed all genes in each individual for two or more NS, SP, or indel variants. We found three to eight candidate genes per individual (Table S2). Among them, only *POLR3B* encoding RPC2, the second largest subunit of RNA Polymerase III (Pol III), was common in two individuals (individuals 1 and 3). The inheritance of the variants in *POLR3B* (transcript variant 1, NM_018082.5) was examined by Sanger sequencing. In individual 1, we confirmed that a canonical splice-site mutation (c.1857-2A>C [p.Asn620_Lys652del]), 2 bp upstream of exon 18, was

inherited from his father, and that a missense mutation (c.2303G>A [p.Arg768His]) in exon 21 were inherited from his mother (Figure 1A). The two mutations were also present in an affected elder sister (individual 2) but not present in a healthy elder brother. In individual 3, we confirmed that a nonsense mutation (c.1648C>T [p.Arg550X]) in exon 16 was inherited from her father and that a missense mutation (c.2778C>G [p.Asp926Glu]) in exon 24 was inherited from her mother (Figure 1A). The two mutations were not present in a healthy younger brother. To examine the mutational effects of c.1857-2A>C and c.1648C>T, reverse transcription PCR and sequencing with total RNA extracted from lymphoblastoid cells derived from the individuals was performed as previously described.[11] We demonstrated that the c.1857-2A>C mutation caused deletion of exon 18 from the *POLR3B* mRNA (Figures 2A–2C), resulting in an in-frame 33 amino acid deletion (p.Asn620_Lys652del) from RPC2 (Figure 1B). In addition, the mutated transcript harboring the nonsense mutation (c.1648C>T) was found to be expressed at a much lower level compared with the wild-type transcript (Figure 2D). The expression level of the mutated transcript was increased after treatment with 30 μM cycloheximide (CHX),[11] which inhibits nonsense-mediated mRNA decay (NMD), indicating that the mutant transcript underwent NMD (Figure 2D). The two missense mutations (p.Arg768His and p.Asp926Glu) found in the three individuals occurred at evolutionary conserved amino acids (Figure 1B). Among the other candidate genes in individuals 1 and 3, *MSLN* (MIM 601051), encoding mesothelin isoform 1 preproprotein that is cleaved into megakaryocyte potentiating factor and mesothelin, is a potential candidate in the family of individual 1 as its homozygous variant segregated with the phenotype; however, it is expressed in epithelial mesotheliomas, and the mutation affects less conserved amino acid (Table S3). The other candidate genes' variants did not cosegregate with the phenotype. Thus, mutations in *POLR3B* are most likely to cause HCAHC in two families.

In individual 4, in whom no *POLR3B* mutations were found, there were six candidate genes for an autosomal-recessive model. Among them, *POLR3A* (MIM 614258, GenBank accession number NM_007055.3), harboring two missense mutations, appeared to be a primary candidate because it encodes the largest subunit of Pol III (RPC1) (Figure 1A and Table S2). By Sanger sequencing, we confirmed that a missense mutation (c.2690T>A [p.Ile897Asn]) in exon 20 was inherited from his father and that another missense mutation (c.3013C>T [p.Arg1005Cys]) in exon 23 was inherited from his mother (Figure 1A). The two mutations were not present in a healthy younger sister. The two missense mutations (p.Ile897Asn and p.Arg1005Cys) occurred at relatively conserved amino acids (Figure 1B). In total, we found four mutations in *POLR3B* and two mutations in *POLR3A*. Evaluation of the missense mutations by PolyPhen-2 program showed that three mutations (p.Arg768His,

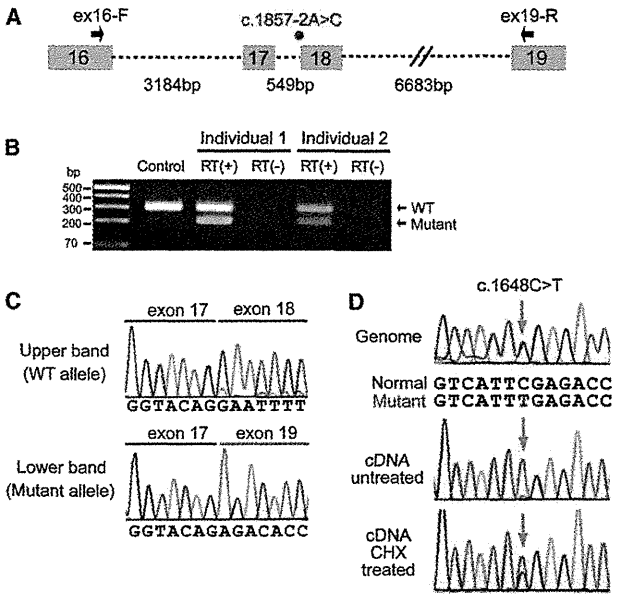

Figure 2. Effects of Splice-Site and Nonsense Mutations in *POLR3B*

(A) Schematic representation of the genomic structure of *POLR3B* from exon 16 to 19. Exons, introns, and primers are shown by boxes, dashed lines, and arrows, respectively. The mutation in intron 17 is depicted as a red dot.

(B) RT-PCR analysis of individuals 1 and 2 with c.1857-2A>C and a normal control. Two PCR products were detected from the individual's cDNA: the upper band is the wild-type (WT) transcript, and the lower band is the mutant. Only a single wild-type amplicon was detected in the control.

(C) Sequence of WT and mutant amplicons clearly showed exon 18 skipping in the mutant allele.

(D) Analysis of the c.1648C>T mutation. Sequence of PCR products amplified with genomic (upper), cDNA from untreated cells (middle), and cDNA from CHX treated cells (lower) as a template. Although untreated cells show extremely low levels of c.1648C>T mutant allele expression, cells treated to inhibit NMD show significantly increased levels of mutant allele expression.

p.Asp926Glu, and p.Ile897Asn) were probably damaging and that p.Arg1005Cys is tolerable. The c.2303G>A mutation (*POLR3B*) was found in one allele out of 540 Japanese control chromosomes. The remaining five mutations were not detected in 540 Japanese control chromosomes, indicating that the mutations are very rare in the Japanese population. Among the other candidate genes in individuals 4, *IGSF10*, a member of immunoglobulin superfamily, is a potential candidate because its variants segregated with the phenotype (Table S3); however, considering a close relationship between *POLR3A* and *POLR3B*, and the fact that *POLR3A* mutations have been recently reported in hypomyelinating leukodystrophy (see below),[12] *POLR3A* abnormality is the most plausible culprit for HCAHC in individual 4.

The structure of Pol III[13,14] and Pol II[15,16] is highly homologous, especially in the largest subunits. Thus, we extrapolated the mutations of RPC1 or RPC2 onto the structure of yeast Pol II (Protein Data Bank [PDB] accession number 3GTP)[17] (Figure 1C). RPB1 and RPB2 subunits of

yeast Pol II are homologous to RPC1 and RPC2 of Pol III, respectively. Asn620_Lys652 in RPC2 corresponds to Tyr679_Lys712 in RPB2. The deletion of Asn620_Lys652 (Tyr679_Lys712) would destroy a structural core of RPB2, leading to loss of RPB2 function. In addition, Arg768 (Arg852 in RPB2) interacts with the main-chain carbonyl group of Arg70 of the RPB12 subunit, and Asp926 (Asp1009 in RPB2) interacts with the side chain of Arg48 of the RPB10 subunit of Pol II (Figure 1D). Arg768His (Arg852His) and Asp926Glu (Asp1009Glu) substitutions are considered to disturb these subunit interactions, leading to dysfunction of the polymerase. Therefore, structural prediction suggests that the mutations in *POLR3B* (RPC2) could affect Pol III function. On the other hand, Ile897 and Arg1005 in RPC1 correspond to Val863 and Arg1036 in RPB1, respectively. Ile897 (Val863) has hydrophobic interactions with Leu170 and Pro176 of the RPB5 subunit and with Phe900 (Phe866) of the RPB1 subunit of Pol II (Figure 1E). Ile897Asn (Val863Asn) substitution is likely to disturb this interaction. Arg1005 (Arg1036) stabilizes interaction between RPB1 and RPB8 subunits (Figure 1F). The Arg1005Cys (Arg1036Cys) substitution appears to make this interaction unstable. Thus mutations in *POLR3A* are also predicted to affect Pol III function.

Clinical features of individuals with *POLR3A* or *POLR3B* mutations are presented in Table 1. MRI revealed high-intensity areas in the white matter in T2-weighted images, cerebellar atrophy, and a hypoplastic corpus callosum in all four individuals (Figure 3). Individuals 1 and 2 showed an extremely similar clinical course. They developed normally during their early infancy, i.e., walking unaided at 15 and 14 months, and uttering a few words at 12 and 13 months, respectively. After the age of 3, individual 1 presented with unstable walking and frequent stumbling and falling down, and individual 2 became poor at exercise. They both had severe myopia (corrected visual acuity of 0.7 and 0.5 at most, respectively). They graduated from elementary, junior high, and high schools with poor records, and the intelligence quotient (IQ) of individual 2 was 52 (WAIS-III). In individual 1, unstable walking was prominent at around 18 years, and he could not ride a bicycle because of ataxia; however, he could drive an automobile. Amenorrhea was noted in individual 2, and was successfully treated by hormone therapy. Individual 1 showed several signs of hypogonadism, including absence of underarm and mustache hair, thin pubic hair (Tanner II), and serum levels of testosterone, follicle stimulating hormone, and luteinizing hormone that were below normal for age 27. Neurological examination of both individuals revealed mild horizontal nystagmus, slowing of smooth-pursuit eye movement, and gaze limitation, especially in vertical gazing, hypotonia, mildly exaggerated deep-tendon reflex (patellar and Achilles tendon reflex) with negative Babinski reflex, and cerebellar signs and symptoms, including ataxic speech, wide-based ataxic gait, dysdiadochokinesis, and dysmetria. Clinical information for individual 3 has been reported previously.[6] Additional findings are as follows: slowing of smooth-pursuit eye movement, gaze limitation in vertical gazing, normal auditory brain responses (ABR), cerebral symptoms with mild spasticity, and intellectual disability (an IQ of 43 according to the WISC-III test), and no myopia but hypermetropic astigmatism. She showed no deterioration besides a mild dysphagia and walks herself to a school for the disabled. Individual 4 developed normally during his

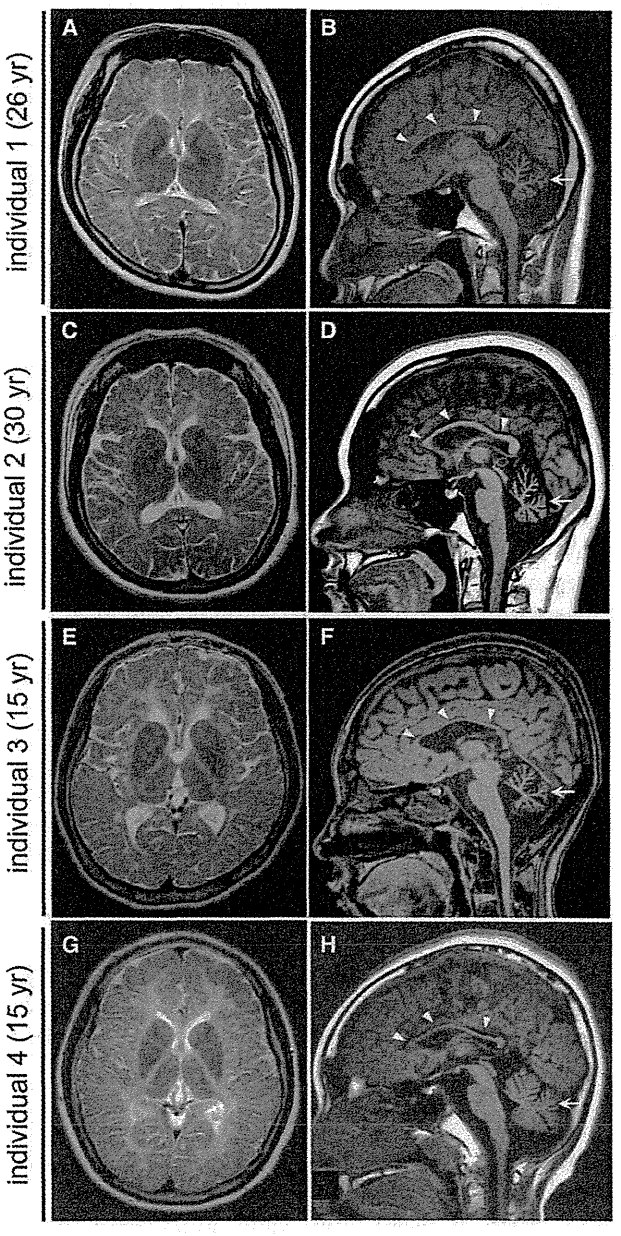

Figure 3. Brain MRI of Individuals with *POLR3B* and *POLR3A* Mutations

(A, C, E, and G) T2-weighted axial images through the basal ganglia. High-intensity areas in the white matter were observed in all individuals.

(B, D, F, and H) T1-weighted midline sagittal images. All the individuals showed hypoplastic corpus callosum (arrowheads) and atrophy of cerebellum (arrows).